The Pennsylvania State University

The Graduate School

Department of Chemistry

THE PHOTOPHYSICS OF ANTHRACENE AND BIANTHRYL AS INDICATORS OF NANOSCALE STRUCTURAL EFFECTS IN ROOM TEMPERATURE IONIC LIQUIDS

A Thesis in

Chemistry

by

Jacob Schesser

Submitted in Partial Fulfillment

of the Requirements

for the Degree of

Master of Science

December 2013

The thesis of Jacob Schesser was reviewed and approved* by the following:

Mark Maroncelli
Professor of Chemistry
Thesis Adviser

John Asbury
Associate Professor of Chemistry

William G. Noid
Associate Professor of Chemistry

Kenneth S. Feldman
Professor of Chemistry
Graduate Program Chair

*Signatures are on file in the Graduate School.

Abstract

The possible effects bulk structure in Room Temperature Ionic Liquids (RTILs) on the photochemistry and spectroscopic behavior of molecular solutes were investigated in relation to chemical reactions in ionic liquids. Anthracene was studied via steady state UV-visible absorption spectroscopy in a series of 1-methyl-3-alkylimidazolium bis(trifluoromethylsulfonyl)imide ($[Im_{n,1}][Tf_2N]$) ionic liquids with alkyl chains of n= 2,4,6,8,10, and 12. Also studied were trihexyltetradecylphosphonium bis(trifluoromethylsulfonyl)imide ($[P_{14,6,6,6}][Tf_2N]$) and mixtures of n-hexane and $[Im_{12,1}][Tf_2N]$. The electron transfer reaction of 9,9'-bianthryl was studied by steady state fluorescence spectroscopy and by time-resolved fluorescence in representatives from the imidazolium series; and in $[P_{14,6,6,6}][Tf_2N]$ and its mixtures with n-heptane.

The spectroscopy of both probes in the liquids studied indicates that they are experiencing a decreased polarity in longer-chain ionic liquids, as would be expected. The trends observed do not seem to point towards significant effects from long-range structure in the liquid.

TABLE OF CONTENTS

Acknowledgements

There are a number of individuals who have provided me a great deal of assistance in a variety of ways during the preparation of this thesis and my graduate career at large. I extend my thanks to Dr. Mark Maroncelli, who taught me most of what I know about molecular spectroscopy and chemical dynamics, and who patiently accommodated my studies in his group over the past two years. Thanks are also due to the members of my committee, Dr. Will Noid and Dr. John Asbury, both of whom have taught me a great deal of chemical physics and have offered a number of helpful suggestions regarding this thesis.

I would also be remiss not to mention those members of the Maroncelli group, current and now former, who have encouraged and assisted me in my studies in one way or another. As such I would like to extend my sincere gratitude to Chris Rumble, Anne Kaintz, Mike Shadeck, Brian Conway, Jens Breffke, Min Liang, and Minako Kondo.

My parents and parents-in-law also deserve many thanks for having been extremely generous in helping me in many regards during the course of my graduate studies. Finally, but certainly not by way of least gratitude, I thank my wife LeighAnna for the patience, love, and encouragement that she has ceaselessly offered to me over the time we have been together, and especially during these past two stressful yet wonderful years.

U.I.O.G.D.

Introduction: Structure in Ionic Liquids and Its Investigation by Various Methods

Chemistry in solution phase differs in many respects from chemistry in either the gas phase or the solid phase. Since many familiar chemical processes, and certainly most of biological significance, do occur in solution, much effort has been expended to understand the effects of the solvent on the process. Many advances in theoretical, computational, and experimental approaches to solution-phase systems have provided a robust framework for explaining such phenomena as solvation dynamics and electron transfer in solution, to name just two. Most of these approaches, however, were formulated in the context of molecular liquids ("conventional" solvents), where the particles of the liquid are electrically neutral and the bulk liquid is homogeneous. In the past decade however, there has been increasing interest in a class of materials known as Room-Temperature Ionic Liquids (RTILs), or simply ionic liquids (ILs). RTILs are substances that are liquid at or below 373K and are completely composed of ions, typically bulky organic cations and inorganic anions. One feature of ionic liquids that makes them attractive for many applications is their tunability, the ability to modify the properties of either or both ions, or select different cation-anion pairs to tune the properties of the liquid to suit particular applications. Very often the main parameter that may be varied for an organic cation within a given family is the length of an alkyl chain. An example is the series of ionic liquids based on 1-alkyl-3-methylimidazolium ions, where the alkyl group in the 1 position may range from ethyl to tetradecyl. In cations with longer alkyl chains, the effect is a polar (charged) "head" portion and a nonpolar (uncharged) "tail" portion, yielding a structure reminiscent of a phospholipid (see Figure 1).

It has been suggested that a consequence of having an RTIL composed of cations with long alkyl groups is the aggregation of the alkyl portions, and segregation of the charged head portions along with the anions, to yield a bulk liquid which exhibits significant structure on the nanoscale. Such structure has been indicated by computational studies of RTILs[1], and has been investigated by such experimental techniques as x-ray and neutron scattering.[2,3] Such scattering experiments so far seem to support the presence of structuring, and indicate that in imidazolium ionic liquids structure begins to appear with

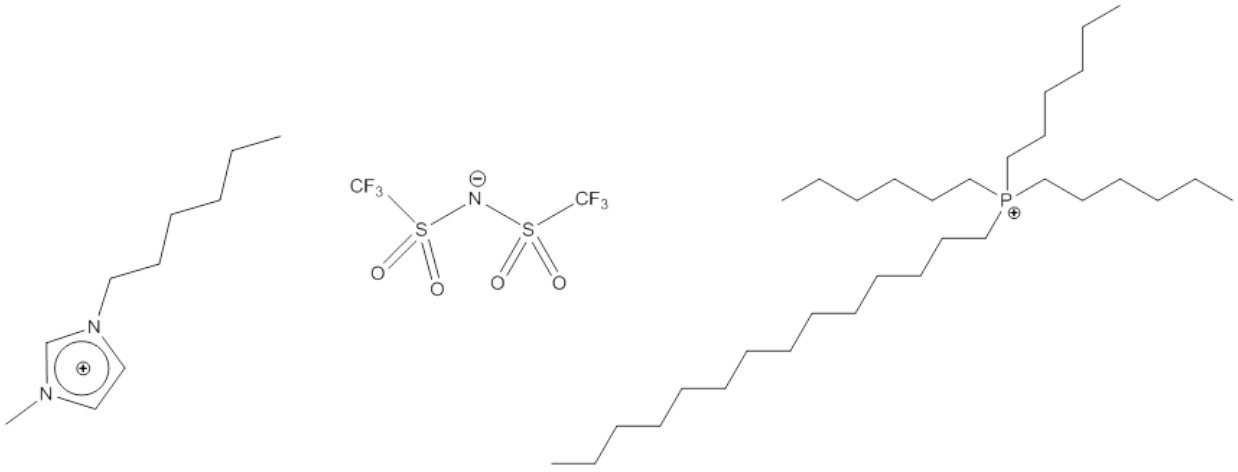

Figure 1: Representative structures of the ionic liquids used in this study. 1-methyl-3-hexylimidazolium cation (left); bis(trifluoromethylsulfonyl)imide anion (center); and trihexyltetradecylphosphonium cation (right).

cation alkyl chain lengths of around n=4.[4] Whereas some workers have even postulated extended lamellar or micellular structures[2,5], others in the field admit that though structure is likely present, such extensive or well-defined morphologies are unlikely.[6,7] Simulation results suggest that the structure found in these liquids is more irregular and intercalated, as shown in Figure 2. There has also been some investigation of the concept of augmenting the native structure of ionic liquids by the addition of co-solvents, typically nonpolar conventional solvents.[4,8] There still remains, however, some debate as to the extent and nature of ionic liquid structure, how the structure of the bulk liquid will be affected by co-solvents, and how a solute molecule or chemical reaction is influenced by this structure, all topics of ongoing interest.

It has been well established that the solvent environment may have a profound effect on a molecule's photochemical and photophysical behavior. Such effects involve perturbations of the energy levels of the molecule in solution, and are therefore often observed spectroscopically as solvatochromic shifts. As these phenomena are dependent upon interaction with the solvent, they may be interrogated to provide information regarding the solvent environment. By extending the observation of such photophysical phenomena into the time-dependent regime by means of ultrafast spectroscopic techniques even greater insight may be obtained regarding the structural and dynamical characteristics of the solvent environment. It is reasonable then to propose using such spectroscopic investigation to examine the structure experienced by small molecule probes in ionic liquids.

The subject of this thesis is the study of the photophysical/chemical behavior of two probes in a series of ionic liquids in an attempt to examine the effect that IL structure has on solutes. The first part of the study is an examination of the bathochromic shift of the anthracene absorption spectrum in a series of imidazolium-based ionic liquids. The second part consists of measuring the dynamics of the intramolecular electron transfer of 9,9'-bianthryl in a series of ionic liquids and mixtures of ionic liquids with other solvents via time-resolved fluorescence spectroscopy. As the dynamics of the reaction are sensitive to environmental effects, they should provide insight regarding structure. The ionic liquids studied included the 1-methyl-3-alkylimidazolium bis(trifluoromethylsulfonyl)imide (abbreviated

[$Im_{n,1}$][Tf_2N], where n is the number of carbons in the alkyl chain with n=2,4,6,8,10,12) and trihexyltetradecylphosphonium bis(trifluromethanesulfonyl)imide ([$P_{14,6,6,6}$][Tf_2N]). The structures of the ILs and probes used in this study may be found in Figures 1 and 3 respectively. This study also investigated the question of the structural augmentation of RTILs by the addition of co-solvents. For this portion of the study, RTILs composed of cations with large alkyl groups ([$P_{14,6,6,6}$] and [$Im_{12,1}$]) were combined with varying amounts of either n-hexane or n-heptane. The effects of this augmentation were tested for both of the probes studied.

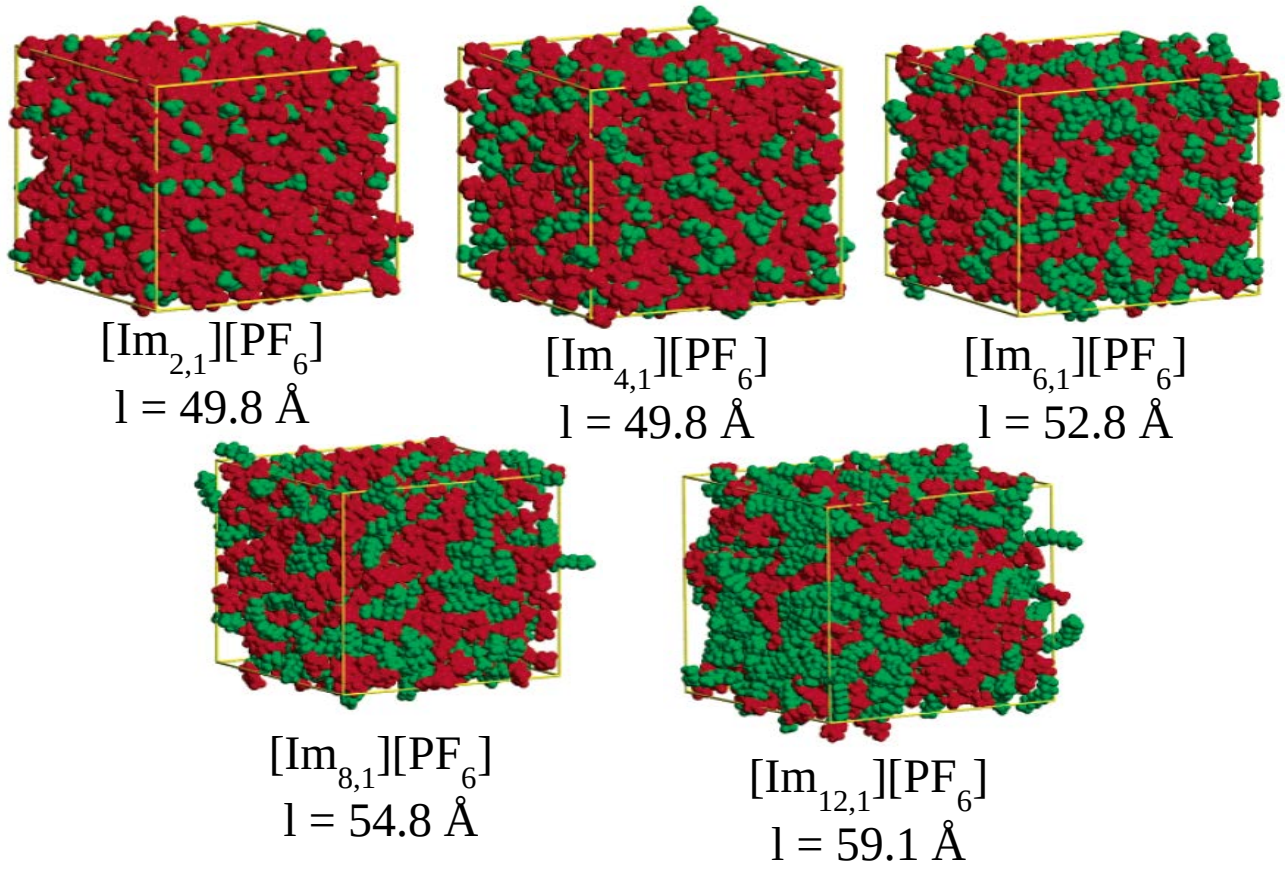

Figure 2: Simulation snapshots showing the predicted morphology of ionic liquid structure in a series of imidazolium hexaflourophosphate liquids. Red areas are the cation heads and anions and the green regions are the alkyl tails of the cations. The values of l are the lengths of the sides of the simulation boxes Adapted with permission from Nanostructural Organization in Ionic Liquids. Canongia Lopes, Jose N.A.; Padua, Agilio A. H. *J. Phys. Chem. B*, **2006**, *110*, 3330. Copyright 2006 American Chemical Society.

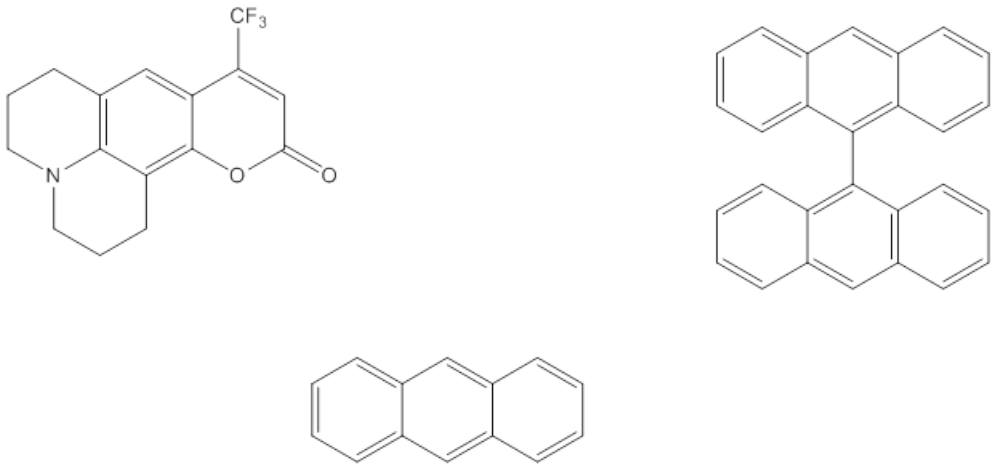

Figure 3: Structures of probes used in this study. Coumarin 153 (top left), the solvation dynamics probe; 9,9'-bianthryl (top right), the electron transfer probe; and anthracene (bottom).

Part I: Bathochromic Shift of Anthracene $S_0 \rightarrow S_1$ Transition as a Probe of RTIL Structure

1. Overview

Anthracene is a polyaromatic hydrocarbon possessing a strong $S_0 \rightarrow S_1$ absorption spectrum in the UV. Whereas the absorption spectra of some probes such as coumarin 153 (C153) are particularly sensitive to the dipolar character of the solvent, anthracene is more sensitive to the electronic polarizability of the solvent.[9] In the present study the interest is primarily in the effect that the changing electronic polarizability due to the increasing alkyl chain length along a series of imidazolium-based ILs will have on the anthracene bathochromic shift. It has been shown by other workers that the functional group contributions to a number of ionic liquid properties, including the refractive index, which is related to polarizability via the electronic field factor $\left(\frac{n^2-1}{n^2+2}\right)$, are additive.[10] It may therefore be expected that increasing the chain length within a family of cations would simply lead to a linear increase in polarizability and therefore a linear bathochromic shift if the solvent were homogeneous. On the other hand, if anthracene is experiencing a predominately alkane-pool environment in a structured IL, a deviation from such a linear trend might be expected. To assess this prediction, the anthracene absorption spectrum was measured in the series of imidazolium ionic liquids with alkyl lengths from ethyl to dodecyl. In order to obtain further insight, mixtures of hexane in $[Im_{12,1}][Tf_2N]$ were prepared. Presumably if alkane-rich regions in a structured IL do exist, the additional alkane would augment these regions, thus extending the structure.

2. Experimental

Solid anthracene which had been previously purified by sublimation was dissolved directly into each solvent studied to obtain a solution with an optical absorbance maximum of ~1.0 for a 2 mm path length. Samples were placed in 2 mm quartz spectrophotometer cuvettes and spectra were collected on a Hitachi U-3000 UV-Visible spectrophotometer. The spectra collected span the region from 345 - 400 nm

with a resolution of 0.1 nm in order to capture the first two major vibronic absorption bands. As a comparison to the IL data, anthracene spectra were also collected in neat alkanes ranging from 2-methylbutane to hexadecane, and in four conventional polar solvents: methanol, acetonitrile, tetrahydrofuran, and dimethyl sulfoxide (DMSO).

To prepare the mixtures of $[Im_{12,1}][Tf_2N]$ and n-hexane, the appropriate quantities of IL and of n-hexane were weighed into a vial, and the mixture was shaken to form the solution.

The refractive index of each ionic liquid and of the $[Im_{12,1}]$/hexane mixtures was measured using an Abbe model 10450 refractometer at the sodium D line, with the sample prisms maintained at 298 K by means of a circulating water bath.

Once the absorption spectra of the anthracene solutions and of the neat ionic liquids were collected, the spectra of the neat IL were subtracted from the anthracene and the spectra were normalized to peak absorbance. The location of the absorption maximum of the spectrum in each solvent was determined by fitting in the custom spectral analysis program *spcany* (written by Dr. Mark Maroncelli), and was then subtracted from the gas-phase absorption maximum (27.621 kcm^{-1}) to obtain the bathochromic shift. Raw anthracene absorption profiles and the absorption of the ionic liquids are shown in Figure 4, where it may be noticed that some ILs in this series, particularly the long-chain cations, exhibit substantial impurity absorption. The solvent-subtracted anthracene spectra in the imidazolium ILs studied, along with three conventional solvents for reference, are presented in Figure 5. These spectra illustrate the fact that anthracene is primarily sensitive to properties other than polarity, as the acetonitrile (MeCN) and n-octane spectra are very close in frequency, even though acetonitrile is much more polar.

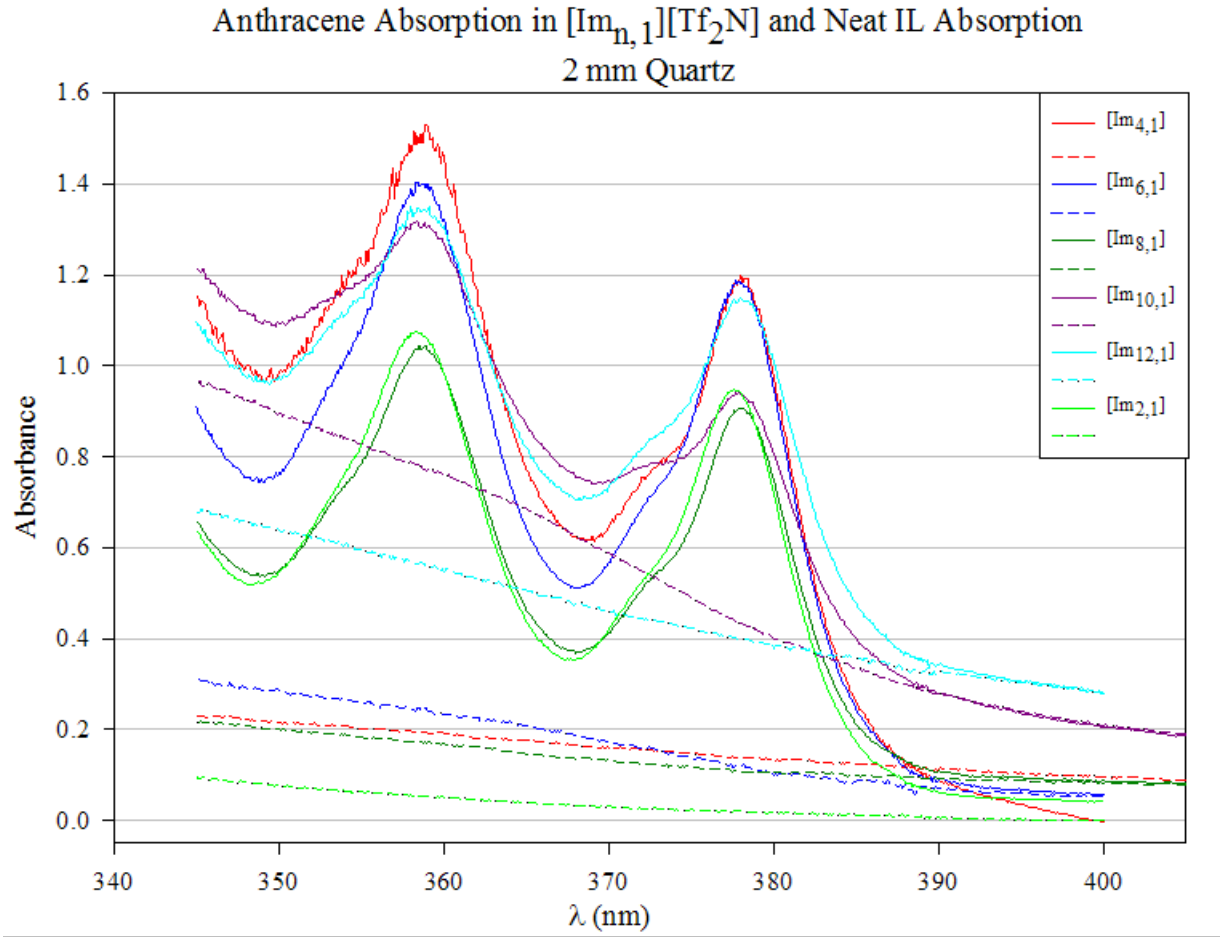

Figure 4: Raw absorption spectra of anthracene in the $[Im_{n,1}][Tf_2N]$ series. The band used to determine the bathrochromic shifts is the lowest energy vibronic finger, near 380 nm. The absorption profiles of the neat ionic liquids (dashed lines) are also shown, indicating the presence of impurities in the liquids.

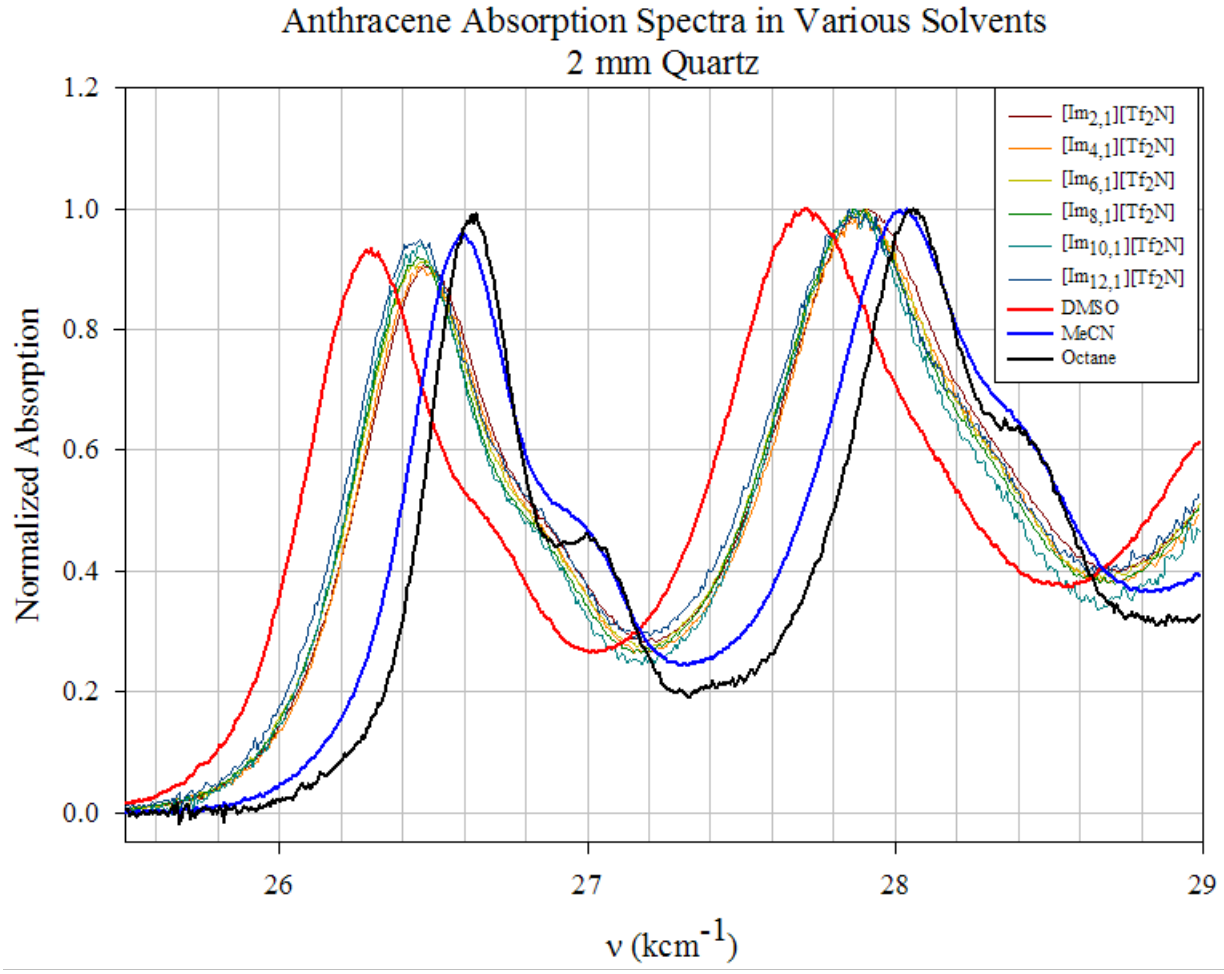

Figure 5: Anthracene absorption spectra in the $[Im_{n,1}][Tf_2N]$ series of ionic liquids, and in three conventional solvents. The solvent absorption spectra have been subtracted and the intensities normalized to the second vibronic peak.

3. Results

The observed bathochromic shifts measured in all of the solvents studied were first plotted versus $\left(\frac{n^2-1}{n^2+2}\right)$ to determine the effect of the electronic polarizability of the solvent (Figure 6). It is seen in the data presented in Figure 5 that though there is a systematic contribution to the bathochromic shifts in all solvents due to electronic polarizability, there is an additional and commensurate contribution in both the polar conventional solvents and the ionic liquids. To more completely account for the dielectric response contributing to the spectral shifts, they are compared to shifts predicted using the following expression[4]:

$$\Delta\nu_{gas\rightarrow solution} = \alpha\left(\frac{n^2-1}{n^2+2}\right) + \beta\left[\left(\frac{\varepsilon-1}{\varepsilon+2}\right) - \left(\frac{n^2-1}{n^2+2}\right)\right] \quad (1)$$

where n is the refractive index of the solvent, ε is its static dielectric constant, and α and β are constants specific to the solute (for anthracene α = 4100 cm^{-1}, β = 170 cm^{-1}) determined by fitting spectra in a wide range of conventional solvents. The second (β) term in Eq. 1 accounts for the orientational polarizability of the solvent. A plot of observed bathochromic shifts versus those calculated using (1) is shown in Figure 7.

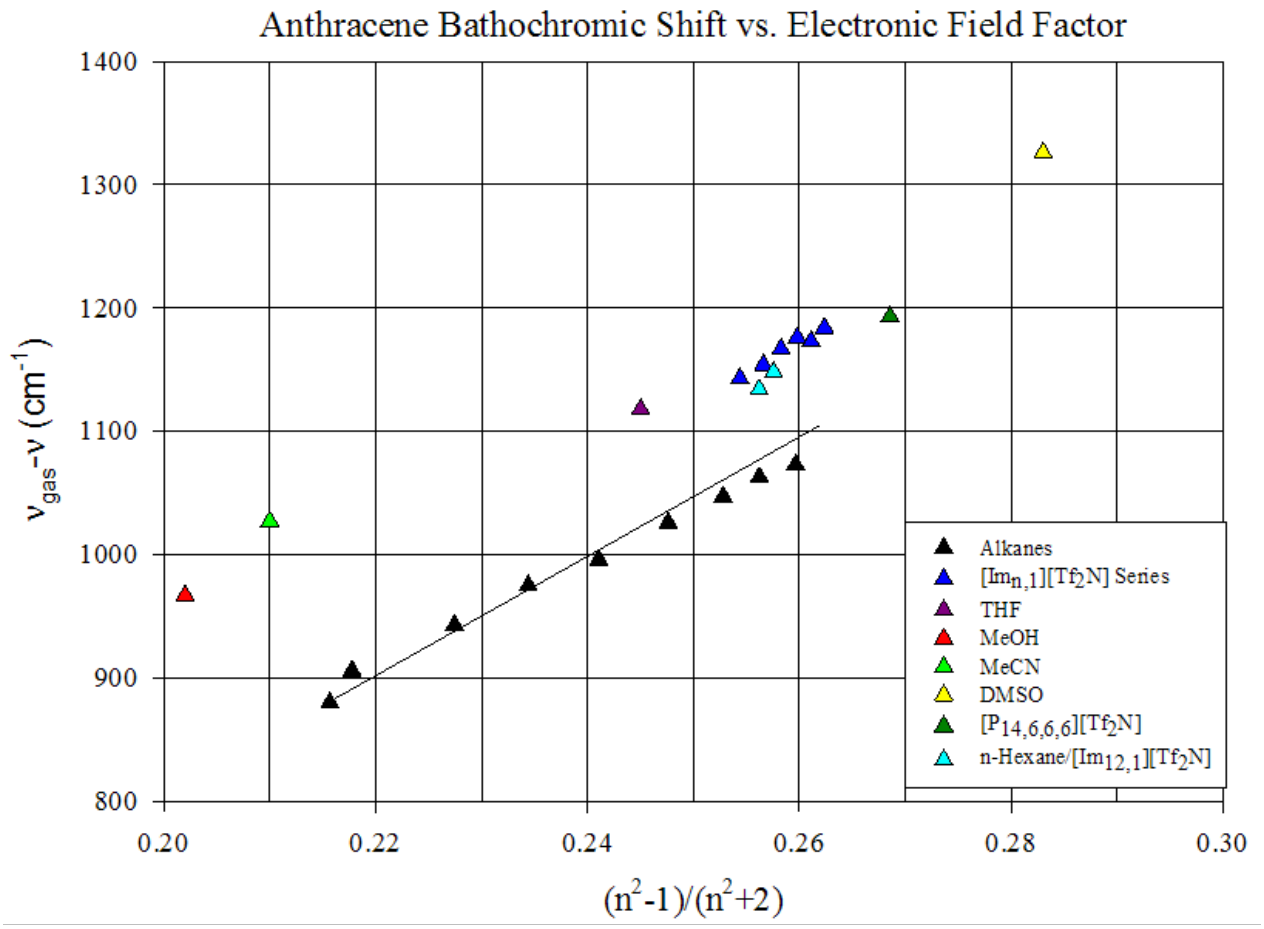

Figure 6: Anthracene absorption shifts plotted as a function of the refractive index field factor illustrating the effect of electronic polarizability on the spectra.

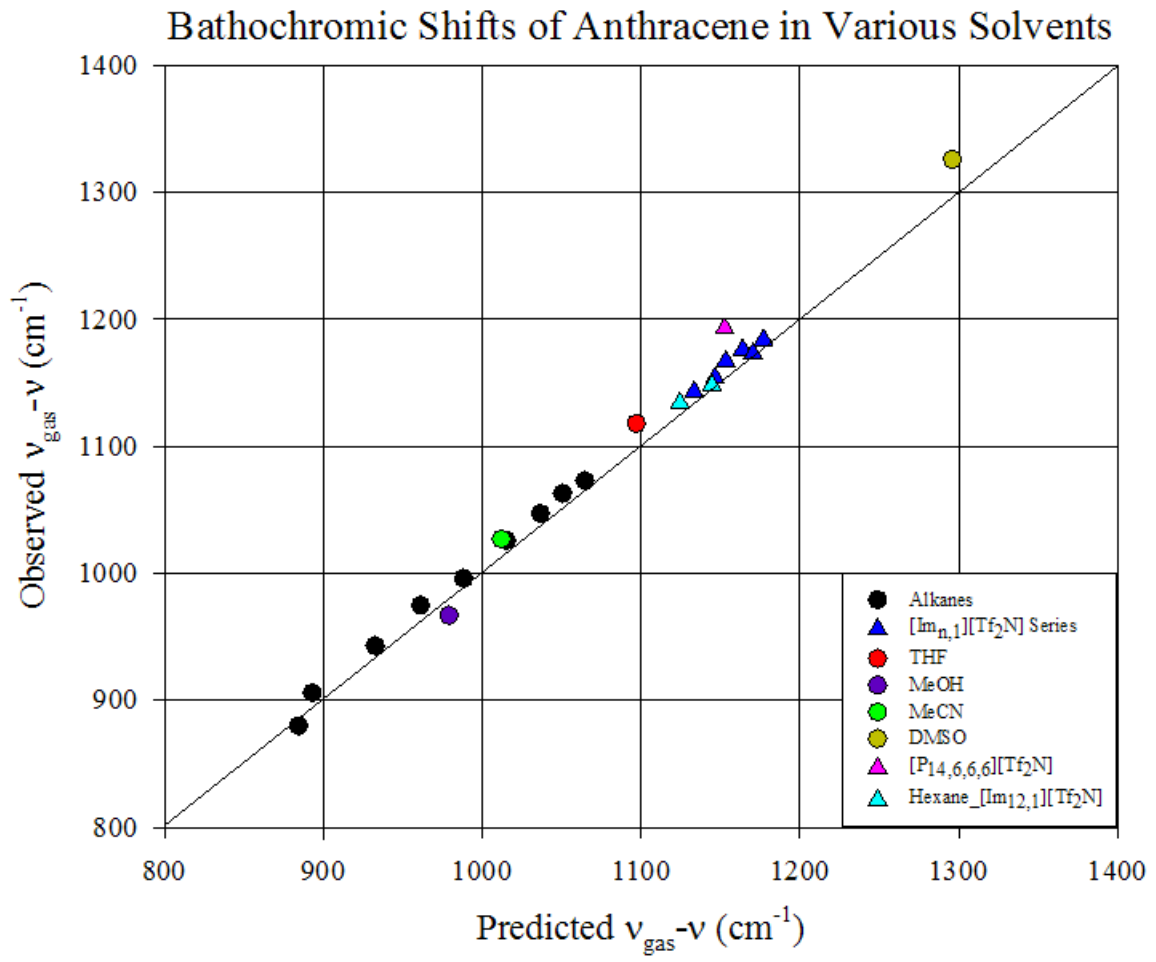

Figure 7: Observed bathochromic shifts of anthracene absorption in a range of conventional solvents and ionic liquids plotted versus the shifts predicted by Eqn. 1

4. Discussion

In comparing Figures 5 and 6, it is clear the shifts of the anthracene absorption spectra in the ionic liquid solvents follow the same general trend as in conventional solvents. As with polar conventional solvents, the orientational polarizability must be included to obtain the complete description of the shift. The strength of the agreement between ILs and conventional solvents shown in Figure 6 suggests that anthracene experiences an averaged environment in the ionic liquid, as if it were dissolved in a very polar conventional solvent, rather than being sequestered in an alkane-like environment. If the probe were reporting on any such extensive structure, it would be expected that some notable deviation from the trend shown in Figure 6 would be observed in ILs with chain lengths exceeding that needed for domain formation (n~6). One caveat however is that, as discussed in Section 3.2 of Part II below, the dielectric response of ionic liquids, typically expressed in terms of ε, is not yet fully understood. So while including a field factor dependent upon ε may result in good agreement with conventional solvents, the physical explanation of this phenomenon may not be as clear.

Part II: Electron Transfer Dynamics of 9,9'-Bianthryl as an Indicator of RTIL Structure

1. Overview

Charge transfer reactions in solution have long been a topic of interest to the physical chemistry community, and with the work of Marcus and others the realization was made that in many cases the interaction between the solvent and the charge transfer system has a profound influence on reaction dynamics. As such, electron transfer dynamics may be interpreted so as to probe select solvent properties.

9,9'-Bianthryl ("bianthryl" or simply "BA" from here on; see Figure 3) is a dimer of anthracene which is known to undergo an intramolecular electron transfer upon photoexcitation in solution. Bianthryl is initially excited to what is referred to as the locally excited (LE) state, corresponding to an $S_0 \rightarrow S_1$ excitation on one of the two anthracene rings. The fact that this excitation is localized (i.e. to one of the two rings) is indicated by the similarity between the absorption spectra of bianthryl and anthracene (see Figures 8 and 9 and discussion thereof). In sufficiently polar solvents, an electron is transferred from one ring to the other, yielding the charge-transferred (CT) state. Both states may be observed spectroscopically as bianthryl exhibits dual emission. As depicted in Figure 8, the fluorescence in nonpolar solvents is completely characterized by the structured asymmetric band due to emission from the LE state, whereas in polar solvents the spectrum is dominated by the nearly Gaussian and highly Stokes-shifted band corresponding to CT state emission. In the latter case, only a small contribution from LE state emission is visible as a high-frequency "foot" in the steady state spectrum (23-26 kcm^{-1}). Much of the previous spectroscopic and computational work on bianthryl has indicated that both LE and CT are limiting regions of a single adiabatic surface. These two regions of the excited state surface are connected along the reaction coordinate, which is primarily the dielectric relaxation of the solvent.

Given that the ET reaction in bianthryl is driven by solvent polarity, that both states are observable in fluorescence, and that the emission spectrum undergoes a large Stokes shift when the ET occurs make bianthryl an attractive probe to report on the local polar environment in an RTIL.

Information about the local polarity experienced by bianthryl could in turn give insight as to the structure of the liquid.

In this study, the electron transfer dynamics of bianthryl were measured in imidazolium-based ionic liquids at the extrema of alkyl chain lengths to determine the effect of chain length on the polarity experienced by bianthryl. A novel feature of this study, as with the anthracene absorption study, is an attempt to enhance the nonpolar domains present in a bulk ionic liquid. To this end, bianthryl dynamics were also measured in solutions of n-heptane in $[P_{14,6,6,6}][Tf_2N]$.

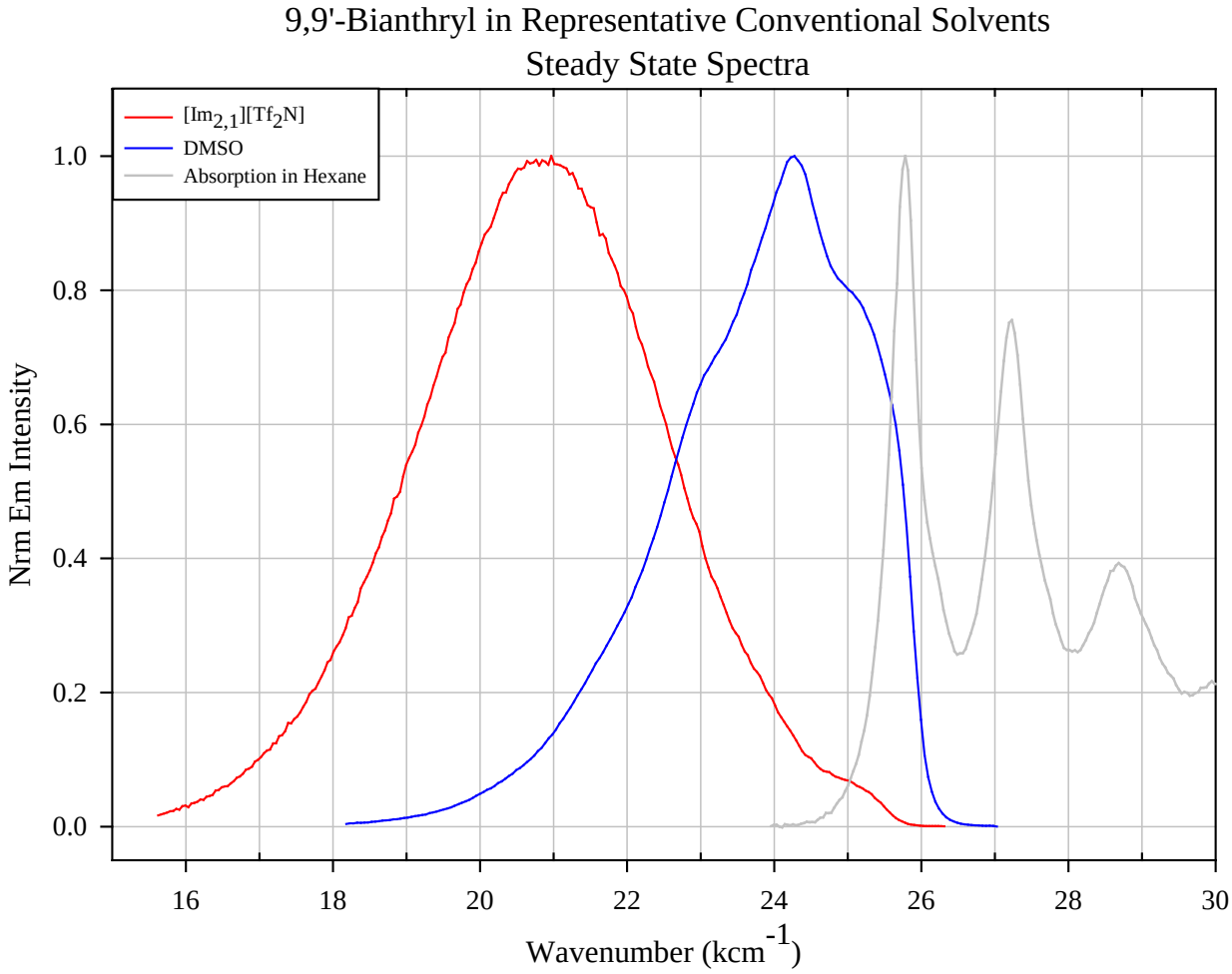

Figure 8: Steady state emission profiles of bianthryl in $[Im_{12,1}][Tf_2N]$ and two conventional solvents solvents. The sample in hexane was excited at 367.5 nm and the DMSO sample excited at 372.5 nm. The emission lineshape in hexane is understood to be entirely due to the LE state. In DMSO the spectrum is dominated by emission from the CT state with only a small contribution from the LE state, visible as the foot at ~25 kcm^{-1}.

2. *Experimental*

The ionic liquids $[Im_{10,1}][Tf_2N]$ and $[Im_{12,1}][Tf_2N]$ were purified by diluting the RTIL with CH_2Cl_2 and stirring over activated carbon for 24-72 hours. The IL/CH_2Cl_2 solution was then decanted off from the carbon and further purified by passing through a column of silica gel. The $[P_{14,6,6,6}][Tf_2N]$ used in this study was prepared from the chloride salt of the $[P_{14,6,6,6}]$ cation as previously described by Li et. al.[11] Solid bianthryl, which had been previously prepared and purified by other workers, was used to prepare a stock solution with an optical density of ~1.0 in spectroscopic grade heptane with a path-length of 1 mm. To prepare the solutions of bianthryl in the ionic liquid solvents, 1 mL of a heptane stock solution was transferred to a vial, the heptane evaporated with streaming nitrogen, and a ~ 1mL portion of the solvent added to dissolve the bianthryl. Spectra were collected in 1 mm path length quartz spectrophotometer cuvettes. The steady state absorption spectra of the bianthryl solutions were collected on a Hitachi U-3200 UV-Visible spectrophotometer in the region between 420 and 320 nm. Steady state fluorescence spectra were collected on a Horiba SPEX Fluorolog fluorimeter with a xenon arc lamp excitation source and Peltier-cooled PMT photon counting detector. Slits were set to 0.6 mm to achieve a spectral resolution of 1 nm. The samples were excited at 380 nm and emission was collected between 390 and 725 nm.

Time-resolved emission for the study of electron transfer dynamics was collected using Time Correlated Single Photon Counting (TCSPC). The TCSPC system used had as the excitation source a Coherent Mira900 Ti:sapphire oscillator pumped by a Coherent Verdi v5 diode laser with an output of 3.95 W. For study of bianthryl electron transfer dynamics, the Ti:sapphire laser was tuned to 760 nm, and the output passed through a β-BaB_2O_4 (β-barium borate or BBO) crystal to double the frequency, giving 380 nm excitation radiation. The 380 nm radiation was passed through an iris, half-wave plate, and polarizer to allow control of excitation intensity before reaching the sample. The sample, in the aforementioned 1mm quartz cuvette, was held in a custom-built cell holder maintained at 298 ±0.2 K by a circulating water bath. The fluorescence emission was focused through a polarizer at magic angle onto a monochromator and subsequent multichannel plate detector.

One difference between these experiments and a typical TCSPC experiment is the use of the front-face (FF) excitation-collection geometry. In a typical fluorescence experiment, a square cross-section cuvette would be used, and the emission collected at a right angle to the excitation beam. In the FF geometry, emission is collected from the same face of the cuvette as the incident excitation radiation. By composing the experiment in this manner much higher concentrations of probe may be used (~1.0 O.D. as opposed to 0.1 O.D. in right-angle geometry). By using higher probe concentrations the relative intensity of probe fluorescence to emission from the solvent is greatly increased, an advantage in the case of ionic liquids which can often have considerable fluorescent impurities. Furthermore, using FF geometry allows the use of smaller cuvettes, reducing the amount of ionic liquid used in an experiment.

The fluorescence decays from the TCSPC experiments were fit to functions of the form

$$I(t) = \sum_{i=1}^{max=4} a_i \exp\left(-\left(\frac{t}{\tau_i}\right)\right) \quad (2)$$

where τ_i is the *i*-th time constant. The fits were performed using the *upcvfit* program written by Dr. Maroncelli. The parameters resulting from these fits were then recorded in a file along with intensities at the corresponding wavelengths of each decay from the steady state emission spectrum. An example of such a file may be found in the appendix. This file was then read into another program written by Dr. Maroncelli, *stokes_analysis*, which facilitates reconstruction of the spectrum and observation of its evolution in time.

Solvation dynamics experiments in $[Im_{12,1}][Tf_2N]$, and in the 0.2 and 0.5 volume fraction heptane in $[P_{14,6,6,6}][Tf_2N]$ mixtures were conducted in essentially the same manner, using C153 as the probe, excited at 400 nm.

3. *Results*

3.1 Comparison of Anthracene and Bianthryl

A cursory comparison of the absorption spectra of bianthryl and anthracene in two solvents, $[Im_{12,1}][Tf_2N]$ and hexane, indicates that the LE state of bianthryl is of the same character as that of anthracene (see Figure 9). These two representative spectra illustrate two important features for understanding the similarity between the two probes. The first is that both probes yield the same basic vibronic band structure. The second is that the bathochromic shifts of the spectra in $[Im_{12,1}][Tf_2N]$ relative to hexane are comparable: 0.24 kcm^{-1} for anthracene and 0.17 kcm^{-1} for bianthryl. Both bianthryl spectra are red-shifted relative to the anthracene spectra due to the inductive effect arising from the appendage of the second anthracene ring. To further illustrate the equivalent absorption behavior and LE state character of bianthryl and anthracene, the bathochromic shifts of bianthryl in the imidazolium series and $[P_{14,6,6,6}][Tf_2N]$ (shifts relative to hexane) are plotted versus the corresponding shifts of anthracene (again relative to hexane) in Figure 10. Overall the shifts appear to linearly correlate with unit slope to a good approximation, though with slight deviations. The negative shift of the trend is, as mentioned above, not unexpected.

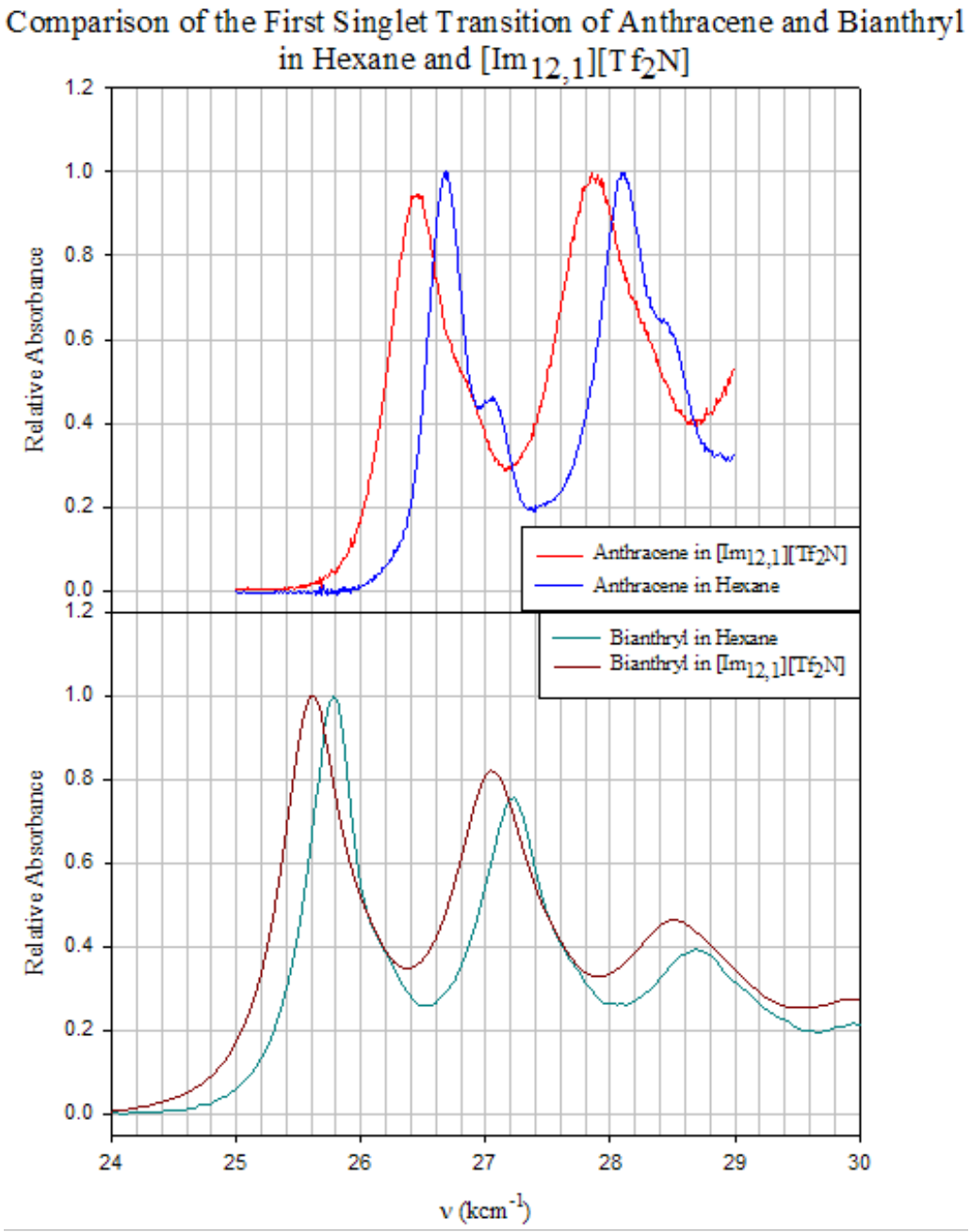

Figure 9: Comparison of the $S_0 \rightarrow S_1$ transitions of anthracene and bianthryl in hexane and in $[Im_{12,1}][Tf_2N]$

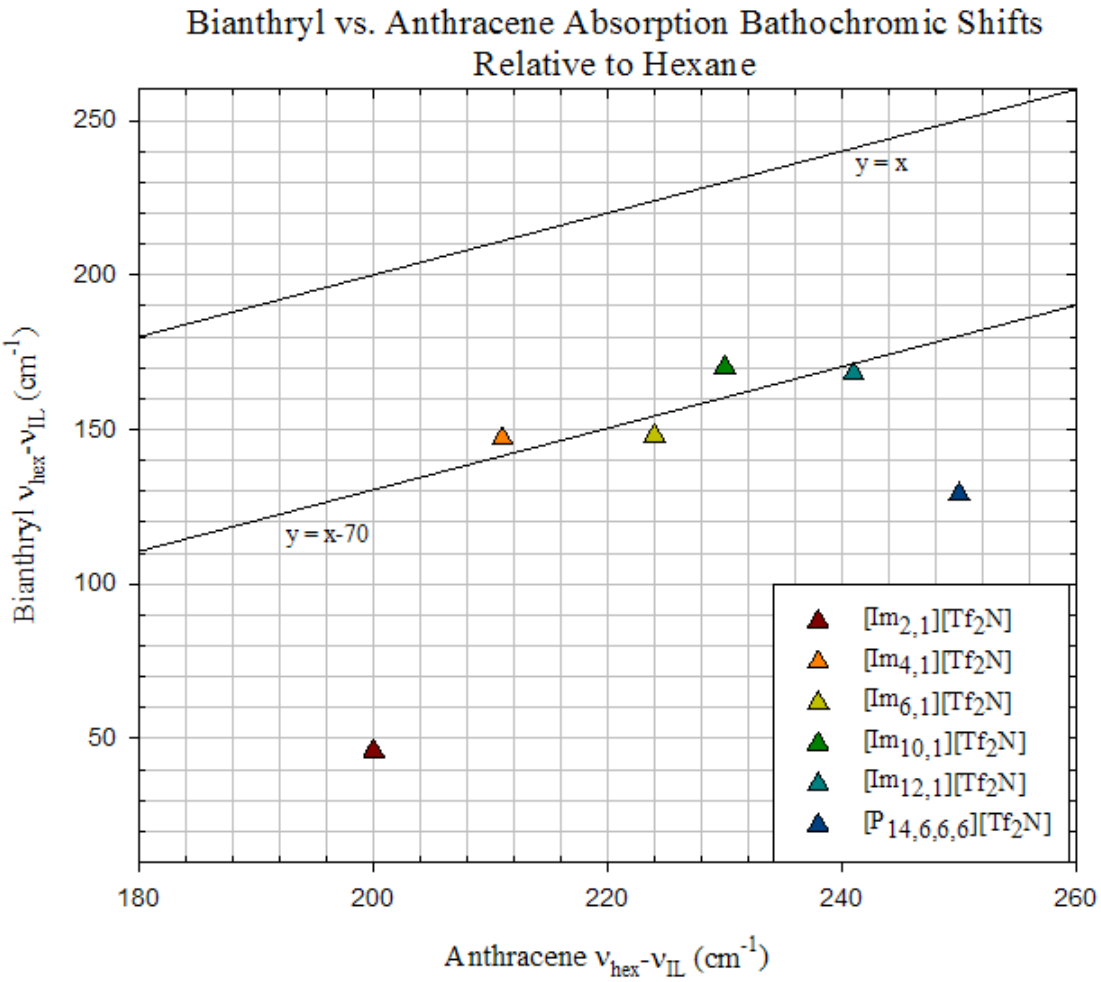

Figure 10: Comparison of the absorption bathochromic shifts ($S_0 \rightarrow S_1$) of bianthryl and anthracene to illustrate the similarity in their absorption behavior.

3.2 Bianthryl Steady State Emission Results

Although a large part of the information regarding the effects of RTIL structure on solutes and reactions comes from the dynamics experiments, much can be learned by considering the steady state spectra as well. The most obvious effect of the solvent on the steady state fluorescence band of bianthryl is the significant Stokes shifting of the CT band, as is clearly illustrated in the series of spectra shown in Figure 11. The greater the ability of the solvent to stabilize charge separation, i.e. the more polar the solvent, the larger the magnitude of the Stokes shift. As such, inspection of the spectra in Figure 10 indicates that $[Im_{2,1}][Tf_2N]$ presents the most polar environment to bianthryl, and that the polarity experienced by this probe gradually decreases with increasing alkyl chain length throughout the imidazolium series. The trend of decreasing polarity continues through $[P_{14,6,6,6}][Tf_2N]$ and its mixtures with n-heptane, although there is a slight apparent anomaly regarding the relative polarity of the mixtures and the neat liquid. The quantity typically used to express the ability of a medium to support charge-separation is the relative permittivity or dielectric constant, ε. In Figure 12 the Stokes shift of the CT band is correlated to the reaction field function of ε for each of the solvents studied here, and to a number of polar conventional solvents in which bianthryl was studied by other workers.[12] The Stokes shift is calculated by subtracting the frequency of the emission spectrum maximum from that of the absorption spectrum. For the liquids studied in this work, the maxima were obtained by fitting the spectra in *spcany*. In the polar conventional solvents the expected behavior of the Stokes shifts is observed, namely a linear increase of the Stokes shift with increasing ε. The data in Figure 8 shows the correlation in ILs deviates profoundly from this trend, and there is furthermore an apparent difference between imidazolium and phosphonium ILs.

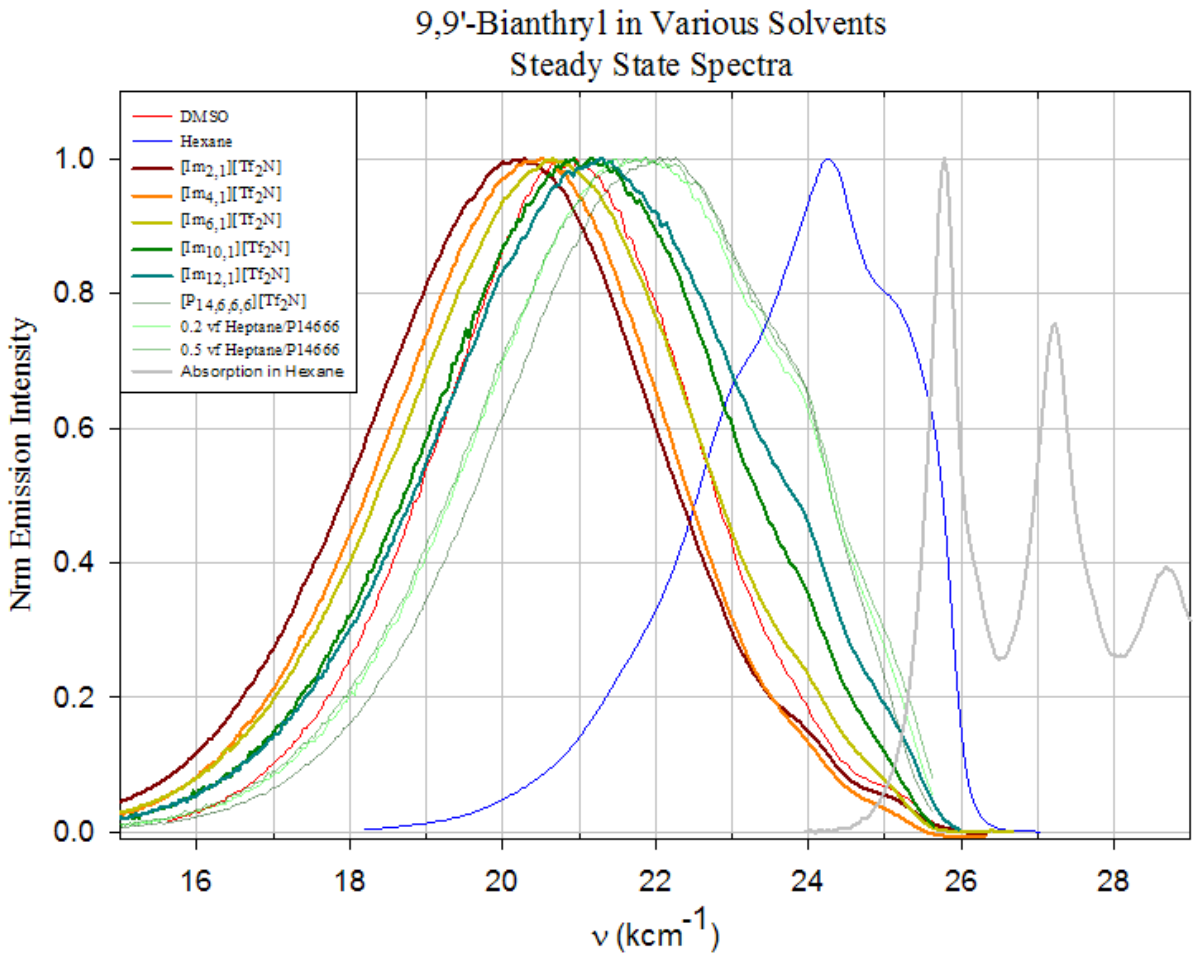

Figure 11: Steady state emission spectra of bianthryl in the series of imidazolium ionic liquids and phosphonium-based mixtures. Emission spectra in conventional solvents and the absorption spectrum in hexane are included for reference. All samples in ILs were excited at 380 nm.

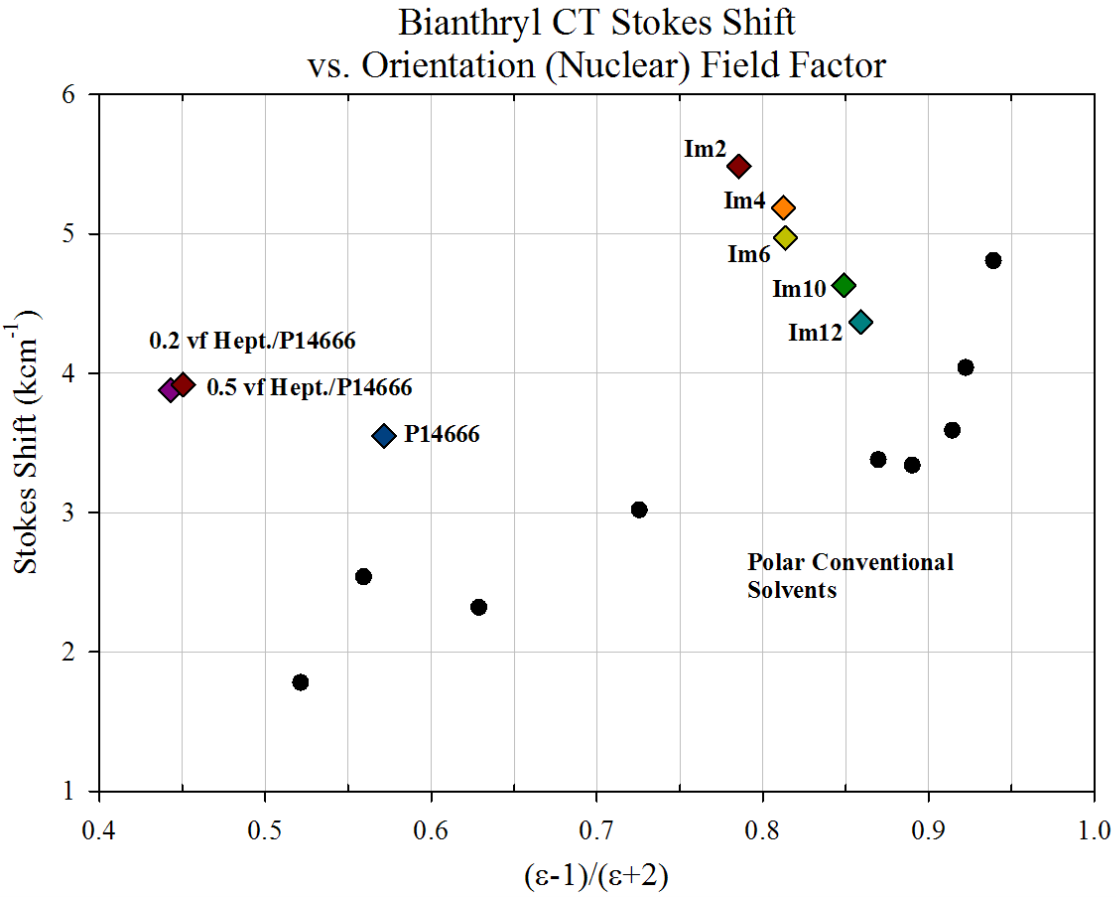

Figure 12: Correlation of bianthryl CT state Stokes shift with a field factor of solvent relative permittivity, ε, in a range of polar conventional solvents and the ionic liquids from this study. The ionic liquid data are the colored diamonds and the conventional solvent data are the black circles.

The seemingly anomalous correlation between the Stokes shift and $\left(\frac{\varepsilon-1}{\varepsilon+2}\right)$ in RTILs is not yet fully explicable. In conventional solvents the dielectric constant sufficiently accounts for the contributing mechanisms of dielectric relaxation, which primarily consist of the orientational motion of solvent dipole moments.[13,14] It may be postulated that in ionic liquids there may be other degrees of freedom that contribute to the dielectric properties of the solvent which are not described by the dielectric constant. Another quantitative description of the polarity of an IL is the ion concentration. Cations with longer alkyl chains will decrease the number of ions that can fit into a given volume, thus effectively diluting the ions. Ion concentrations for the series of ionic liquids in this study were calculated from the molar volumes, V_m, as follows:

$$[Ions] = 2\left(\frac{1000}{V_m}\right) = \frac{mol\ ions}{dm^3} \tag{3}$$

where V_m has units of cm^3/mol. Molar volumes for the imidazolium series and for $[P_{14,6,6,6}][Tf_2N]$ tabulated in the literature[15] were used to calculate the ion concentrations. An apparent linear correlation exists between the Stokes shift of both the C153 band and the CT band of bianthryl, and ion concentration as shown in Figure 12. The relative responses of bianthryl and C153 are further compared by showing the bianthryl Stokes shift in the series of solvents versus those of C153 in Figure 13, which indicates that bianthryl, in the charge-transferred state, is has a greater dipole moment and is thus more sensitive to the local solvent environments. The strong correlation of the BA Stokes shift to that of C153 indicates that the Stokes shift of a polar fluorophore is a good empirical indicator of solvent polarity, which in the case of ionic liquids is still in want of a complete microscopic description.

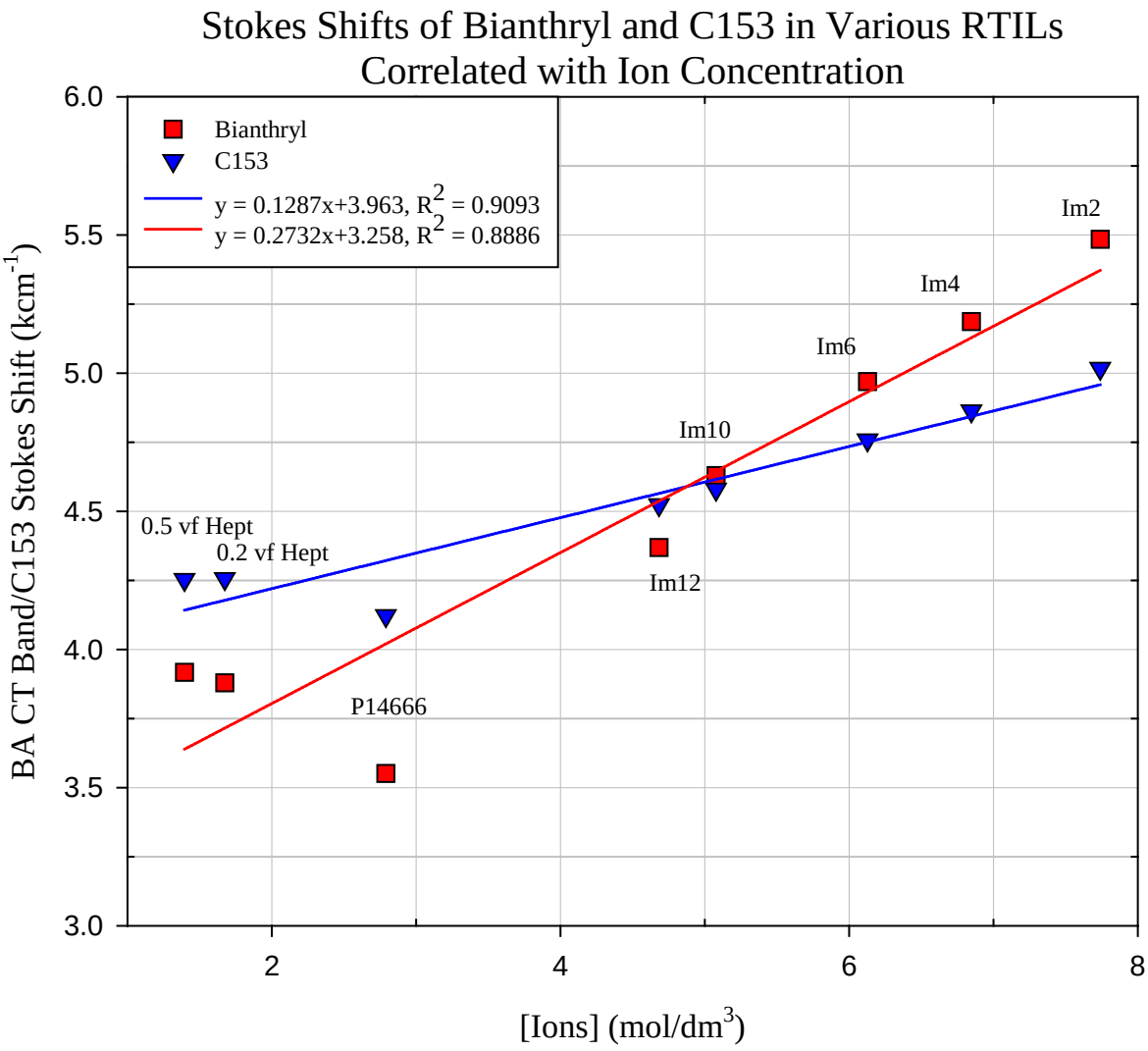

Figure 13: Stokes shifts of the C153 emission band and of the bianthryl CT state band plotted versus the ion concentration.

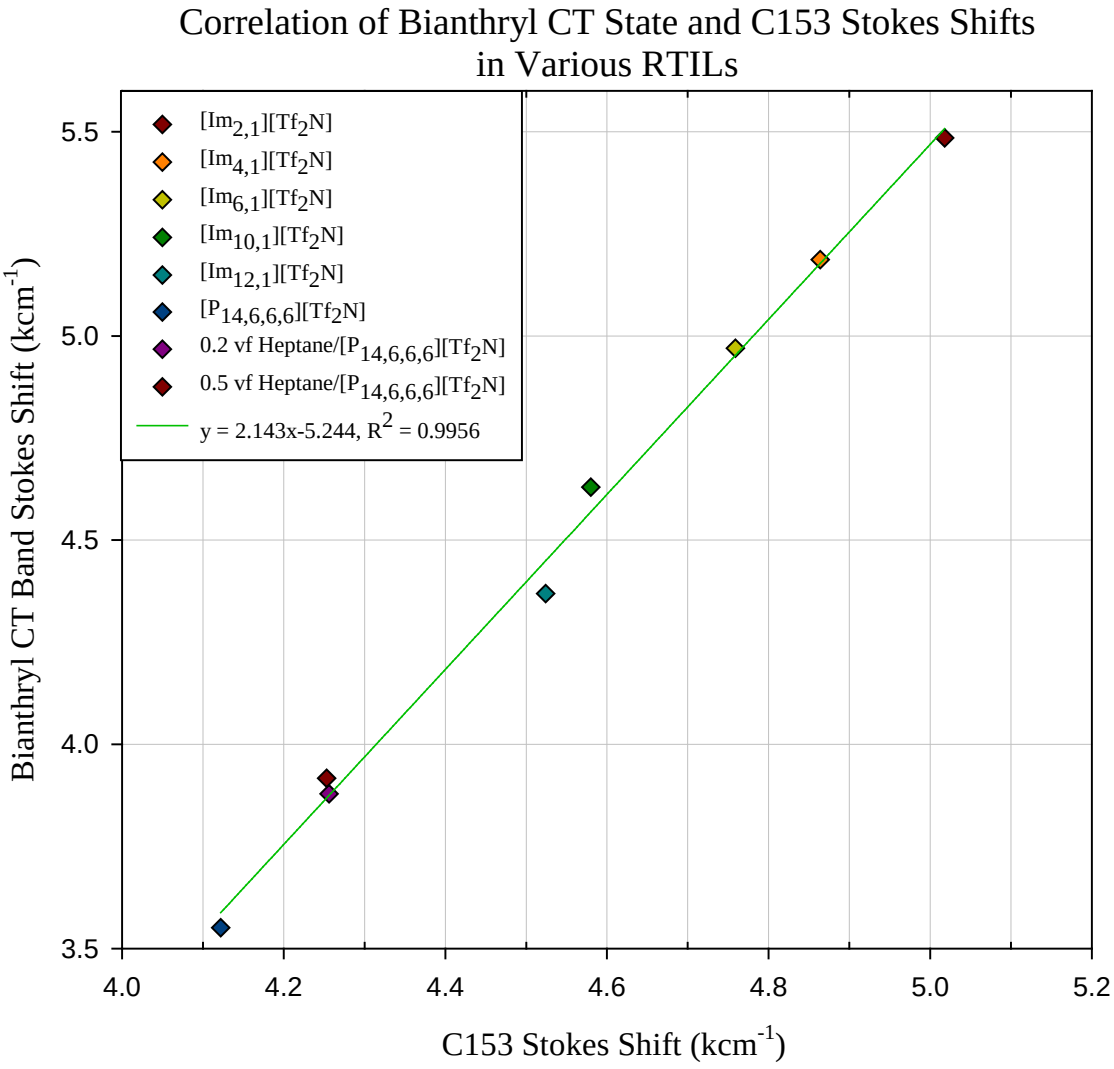

Figure 14: Bianthryl CT band Stokes shift plotted versus the C153 Stokes shift.

In addition to the Stokes shifts, another feature of the steady state spectra which may be quantified is the relative contribution to the total band profile from LE and CT state emission and the trend in the relative contributions through the series of ILs. This feature may be observed qualitatively in the spectra shown in Figure 10. It is possible to quantitatively determine the fractions of LE and CT character by fitting these sepctra to a sum of the hexane spectrum (which is completely of LE character) with its vibronic structure retained, and a shifted and convoluted hexane spectrum to account for the LE and CT state contributions respectively. Representative spectra and their decompositions are shown in Figure 15. The fractions of LE and CT state contribution may be further employed to calculate a quasi-equilibrium constant for the LE → CT conversion.[16] This constant is taken to be $K = \frac{f_{CT}}{f_{LE}}$, where f_{CT} and f_{LE} are the fractions of LE and CT emission in the total band. A correlation of the natural logarithm of the equilibrium constant with ion concentration again exhibits a linear relation shown in Figure 16. By plotting $\ln(K_{ET}')$ as a function of the CT state Stokes shift, it is again apparent that the Stokes shift is a good empirical indicator of the solvent polarity (Figure 17). In either relation, the trend of increasing equilibrium constant with decreasing alkyl content is consistent with the Stokes shift considerations discussed above.

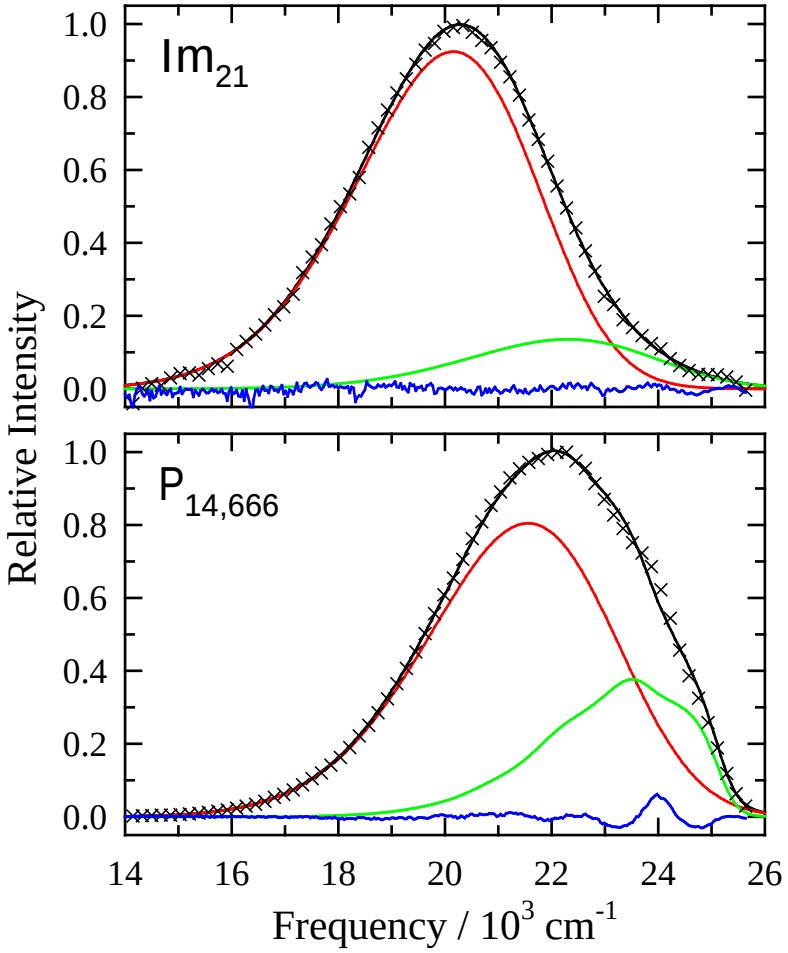

Figure 15: Steady state emission spectra (black lines and Xs) in $[Im_{2,1}][Tf_2N]$ and $[P_{14,6,6,6}][Tf_2N]$ along with LE (green line) and CT (red line) components from fitting. Residuals from the fits (blue lines) are also depicted.

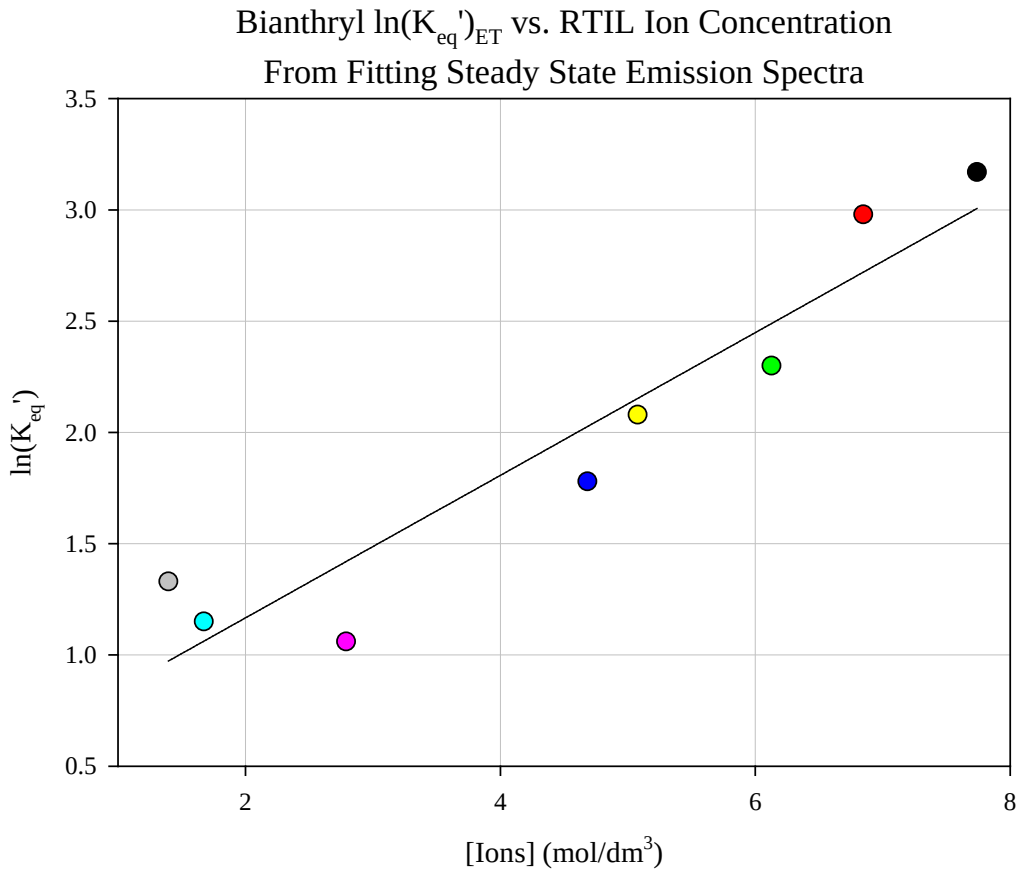

Figure 16: Correlation of the pseudo equilibrium constant, K_{eq}', with RTIL ion concentration

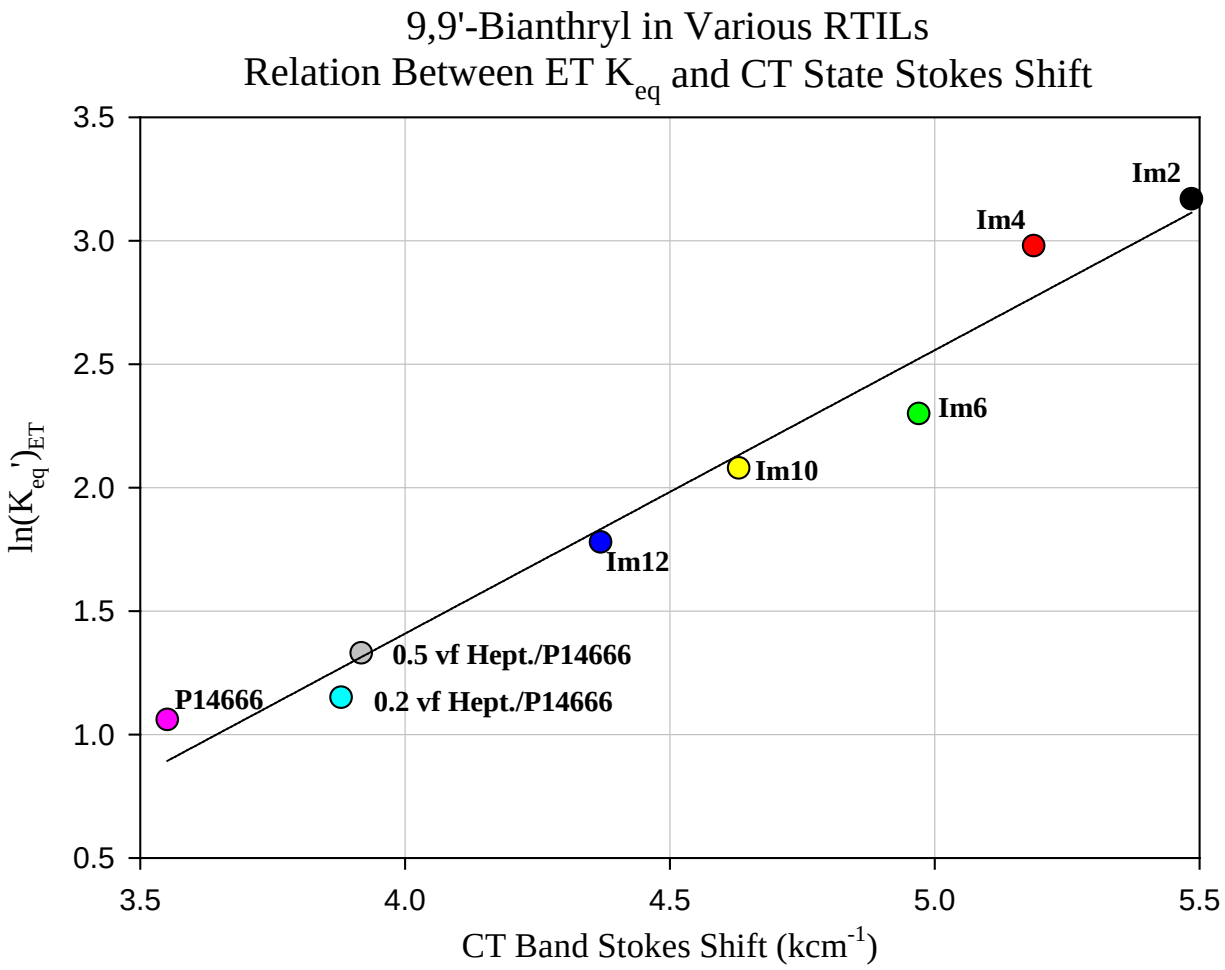

Figure 17: Plot of ln(Keq') for bianthryl as a function of the CT band Stokes shift, an empirical measure of polarity.

3.3 Bianthryl TCSPC Results

The TCSPC experiments with bianthryl were conducted in $[Im_{2,1}][Tf_2N]$, $[Im_{10,1}][Tf_2N]$, $[Im_{12,1}][Tf_2N]$, $[P_{14,6,6,6}][Tf_2N]$, and in mixtures of 0.2 and 0.5 volume fraction n-heptane in $[P_{14,6,6,6}][Tf_2N]$. An example of a series of reconstructed spectra of BA in $[Im_{12,1}][Tf_2N]$, as a function of time, is shown in Figure 18. It may be observed in these spectra that ~50% of the initial intensity decays by 200 ps, and that an observable Stokes shift is present by 1 ns. The same spectra are shown in Figure 19 on a frequency basis and area-normalized to allow observation of potential iso-emissive points, which would be indicative of a two-state process.[17,18] As is consistent with previous studies in conventional solvents, a clear isoemissive point is not observed in the bianthryl spectra collected in any of the ionic liquids studied in this work, although there is a "constriction" near 22 kcm^{-1}. The reason is that relaxation in bianthryl does not involve two distinct states, rather the character of the S_1 state changes continuously throughout the course of the relaxation.

A prediction of the emission spectrum before relaxation begins may be constructed by applying shift and inhomogeneous broadening parameters determined using a reference absorption and emission spectrum in a nonpolar reference solvent. This time-zero spectrum is an estimate of how the emission would be expected to appear before any solvation or photochemistry occur.[19] An example of a time-zero spectrum for $[Im_{12,1}]$ is included in Figure 19. It is apparent based on the differences between the estimated time-zero spectrum and the observed "time-zero" spectrum that the very early stages of the relaxation are not captured by the TSCPC technique, and indeed it is worth mentioning that previous work with bianthryl has suggested that close to 50% of the overall fluorescent decay may be missed in such an experiment[11]. Nonetheless it is presumed that these data are sufficient to determine relation of the LE/CT equilibration lifetime to the solvation time, as both are measured with the same time resolution.

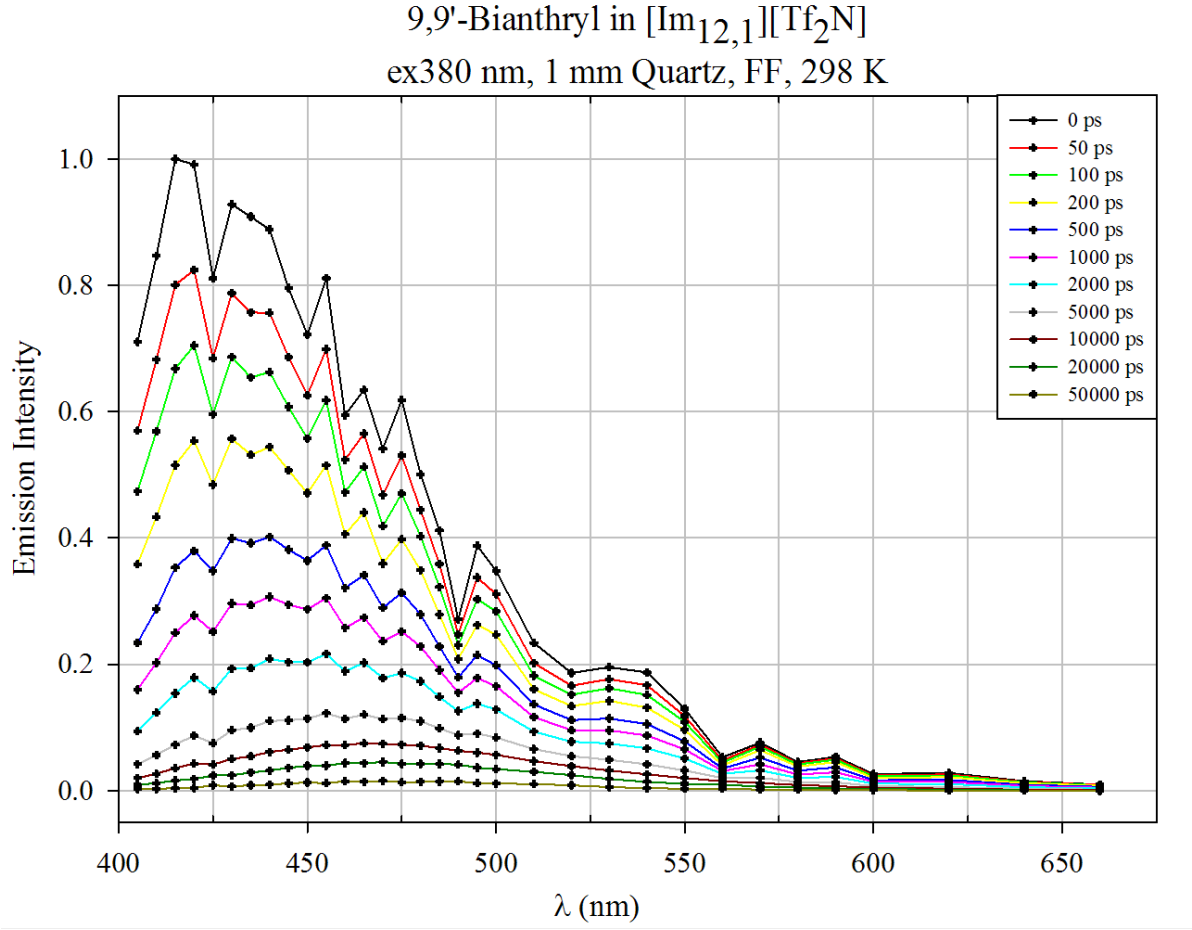

Figure 18: Series of reconstructed spectra of bianthryl in $[Im_{12,1}][Tf_2N]$ at selected times. The symbols indicate the wavelengths at which fluorescence decays were collected.

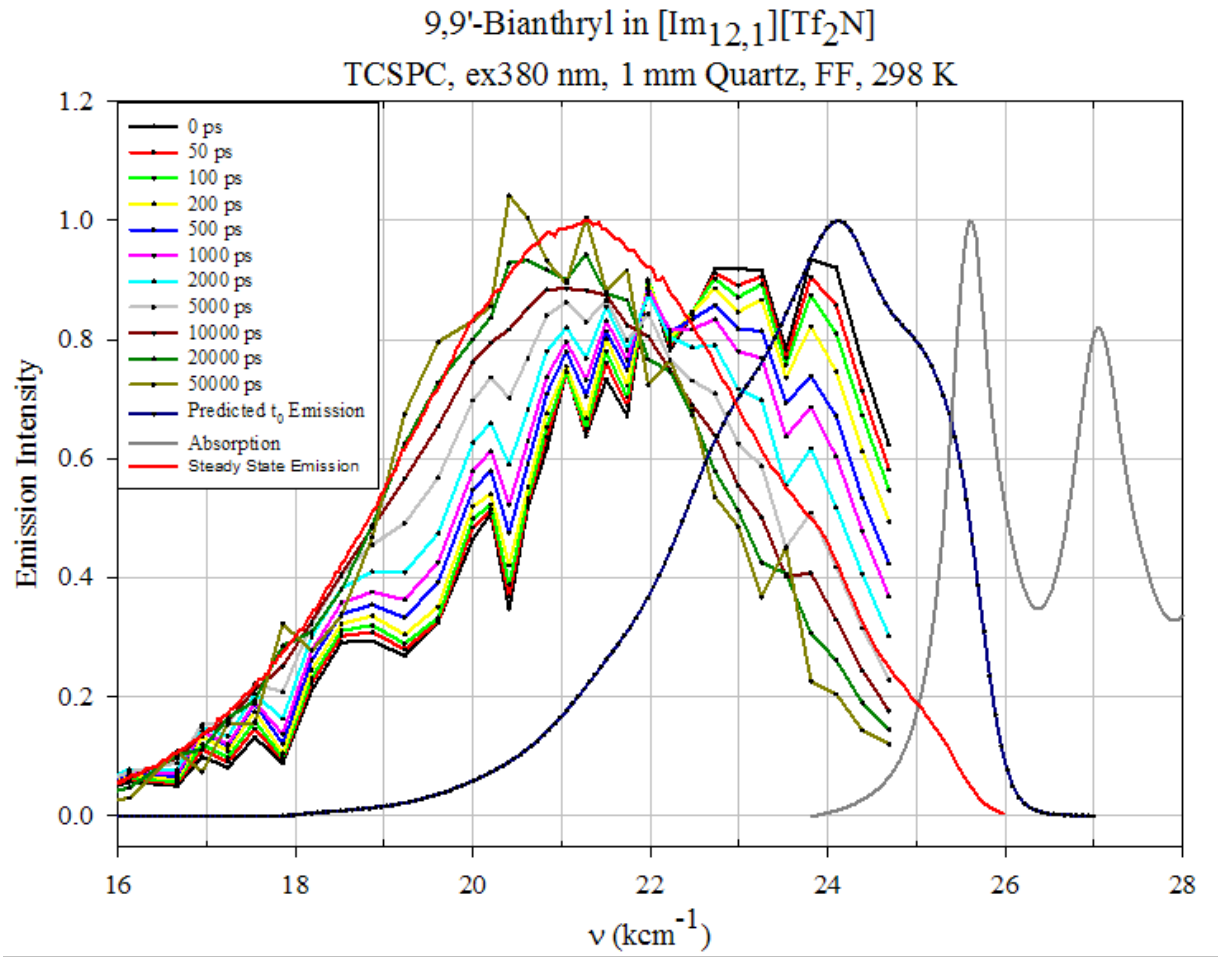

Figure 19: Area-normalized emission spectra of bianthryl in $[Im_{12,1}][Tf_2N]$ at selected times. The predicted time-0 emission, steady state emission spectrum, and absorption spectrum have been overlaid for comparison.

It is informative to first consider qualitatively the behavior of the reconstructed emission spectra in time. The $[Im_{2,1}][Tf_2N]$ reconstruction (Figure 20) shows that even at the shortest times accessible to these experiments (~25 ps), most of the LE character is absent and the emission profile is that of the CT state. In the longest chain imidazolium IL studied, $[Im_{12,1}][Tf_2N]$ (Figure 19), there appears to be a more equal contribution from LE and CT states, even at early times, and a more persistent appearance of the LE shoulder around 24 kcm^{-1} in the steady stare spectrum. Both $[Im_{2,1}][Tf_2N]$ and $[Im_{12,1}][Tf_2N]$ stand in contrast to the mixture of 0.2 volume fraction of heptane in $[P_{14,6,6,6}][Tf_2N]$ (Figure 21), where the spectra at times up to about 2 ns are largely characterized by LE emission, with a fairly abrupt shift to CT character between 2 and 5 ns. These spectral characteristics would seem to indicate that in going from short to long-chain imidazolium ILs, and then to heptane-augmented phosphonium-based liquids, the bianthryl is sensing a progressively less polar environment. While potentially suggestive, this fact in itself is not sufficient to speak conclusively for or against significant structural effects.

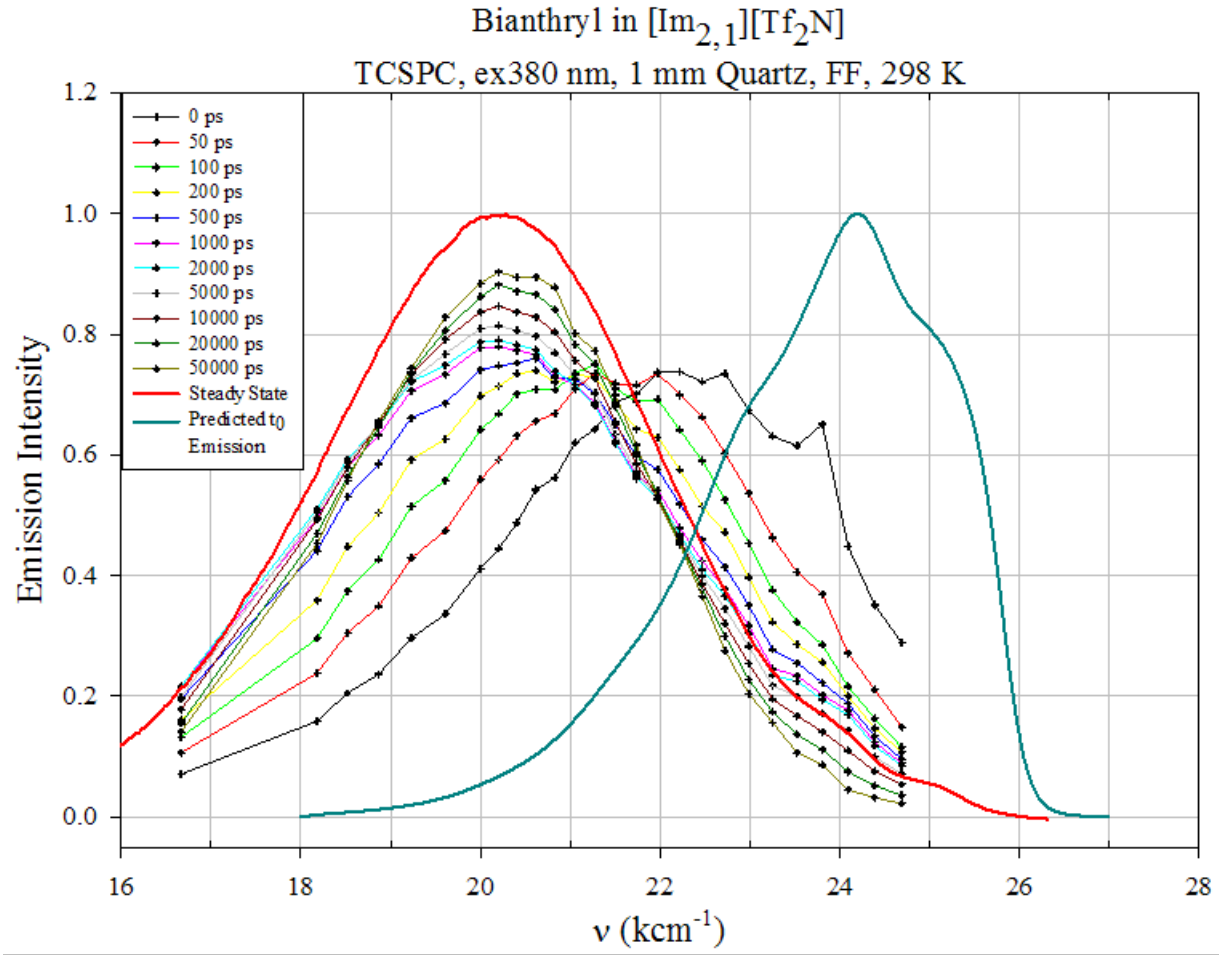

Figure 20: Evolution of the emission spectrum on bianthryl in $[Im_{2,1}][Tf_2N]$, along with the predicted time-zero spectrum and the steady state spectrum.

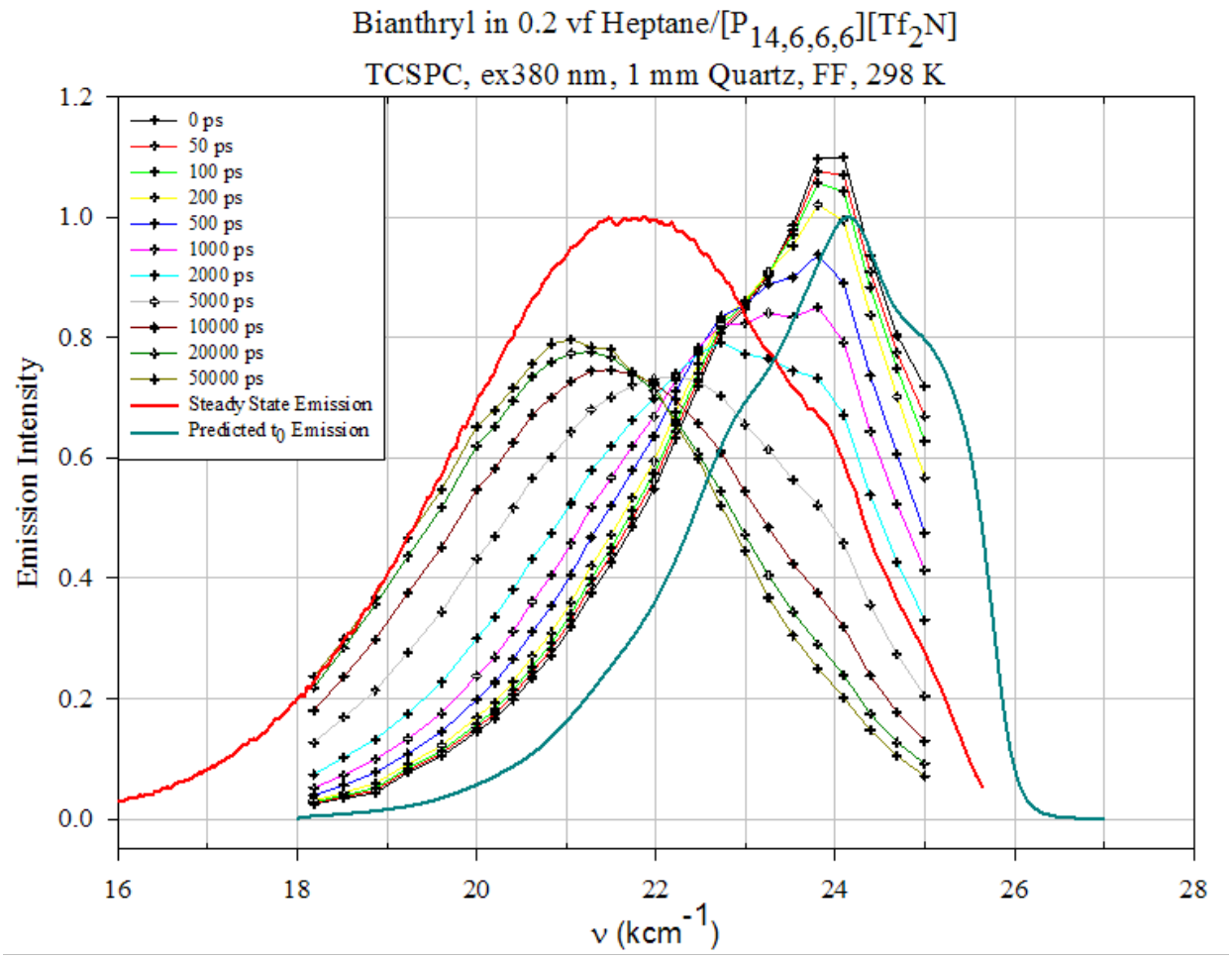

Figure 21: Evolution of the emission spectrum of bianthryl in a 0.2 volume fraction solution of n-heptane in $[P_{14,6,6,6}][Tf_2N]$, with the steady state emission spectrum and the predicted time-0 spectrum overlaid.

By fitting a series of reconstructed spectra to lognormal functions the peak and integral fluorescence intensities, and the peak and average frequencies can be determined as functions of time. By plotting these output data and fitting them, the dynamics of the electron transfer reaction may be determined. A plot of representative data along with the lognormal fits are displayed in Figure 22 to illustrate the agreement of the lognormal fit with the data, and thus the rationality of using such fit functions as a basis for determining dynamics. The entire series of log normal functions for $[Im_{12,1}][Tf_2N]$ is shown in Figure 23. For contrast, the reconstructed and fit series for C153 in $[Im_{12,1}][Tf_2N]$ is also included (Figure 24). By comparing these two series of fit spectra, the "constriction" of the bianthryl spectra discussed above may be seen in clear contrast with the monotonic decay of intensity in the C153 spectra. The integral intensity was fit to a function of the following form:

$$I(t) = c\left[a_1 exp\left(-\left(\frac{t}{\tau_1}\right)^{\beta}\right) + (1-a_1)exp\left(-\left(\frac{t}{\tau_2}\right)\right)\right] \quad (4)$$

In the above equation, c and a_1 are real constants, β is the stretching factor of the stretched exponential term constrained such that $0.3<\beta<1$, and τ_1 and τ_2 are time constants. The first term accounts for the faster portion of the relaxation, which is taken to correspond to the equilibration between the LE and CT states of bianthryl. The second term accounts for the continued $S_1 \rightarrow S_0$ relaxation of the system after the LE/CT equilibrium has been established. As the fast portion of the relaxation is best represented by a stretched exponential function, the dynamics are characterized by a distribution of rates as opposed to a single rate.[20] In order to obtain an average lifetime from these data, the lifetime from fitting to (2) is weighted with respect to β via the following expression: $\langle \tau_{rxn} \rangle = \frac{\tau_1}{\beta}\Gamma\left(\frac{1}{\beta}\right)$, where Γ is the gamma function. Such distributed dynamics result from the collection of probe molecules experiencing a distribution of slightly-varying environments, and may be due to bulk structural heterogeneity or slow, partial relaxation in viscous media. The parameters resulting from fitting the intensity decays to this function may be found in Table 1. The decay data along with the fits for the imidazolium and the phosphonium ILs are shown in Figures 25 and 26 respectively.

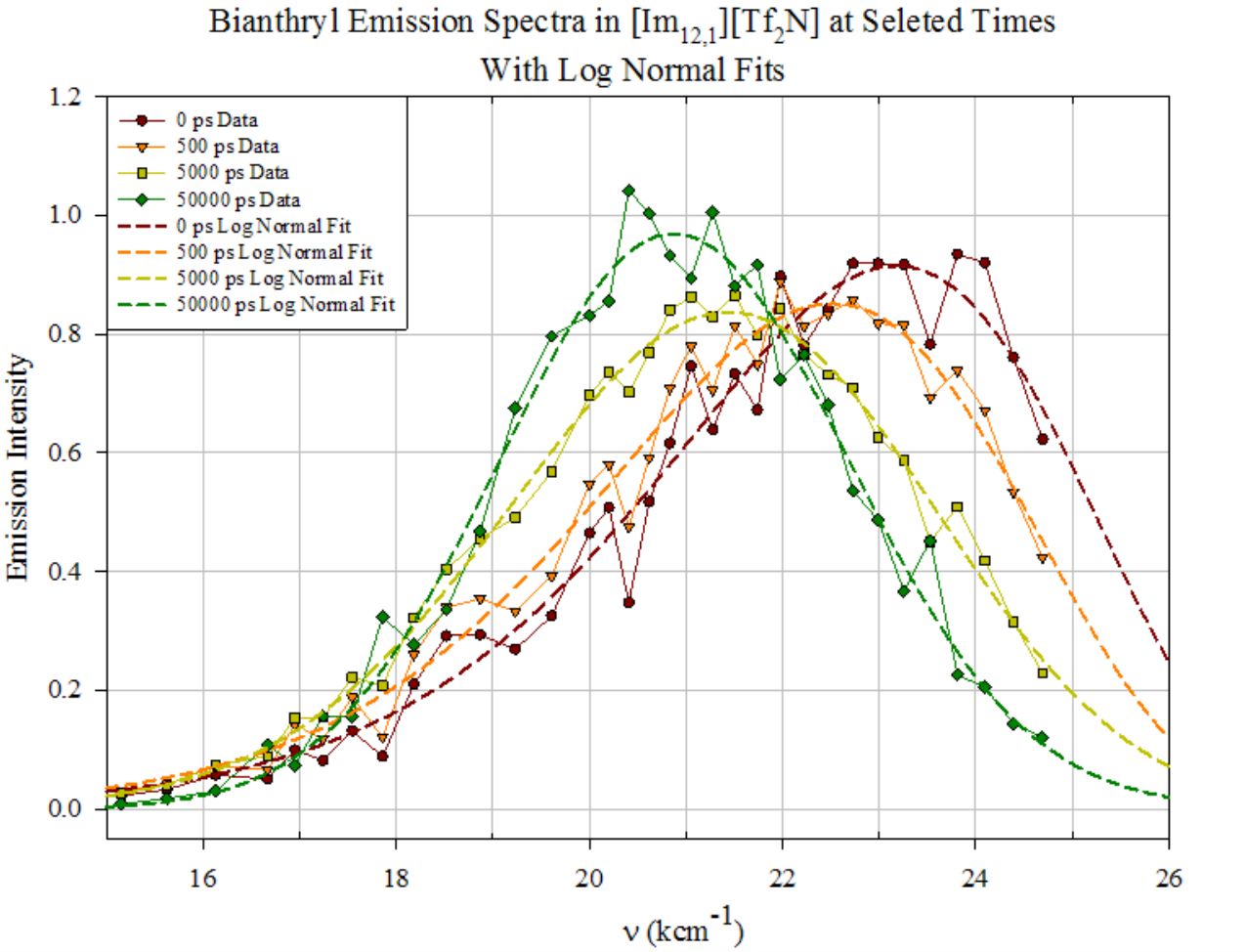

Figure 22: Reconstructed spectra at selected times from TCSPC decays of bianthryl in $[Im_{12,1}][Tf_2N]$ along with lognormal fits.

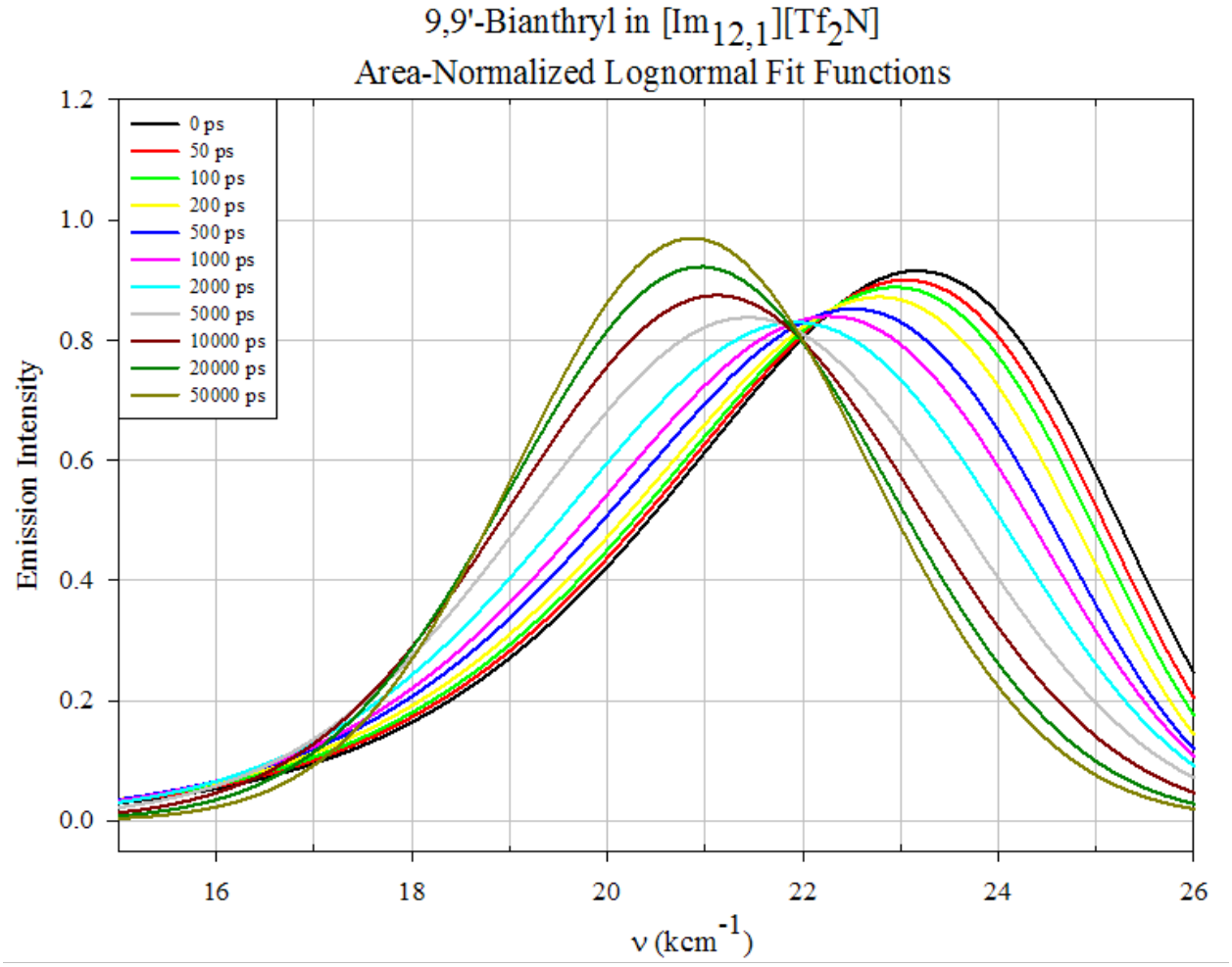

Figure 23: Series of lognormal functions fit to the TSCPC data for $[Im_{12,1}][Tf_2N]$.

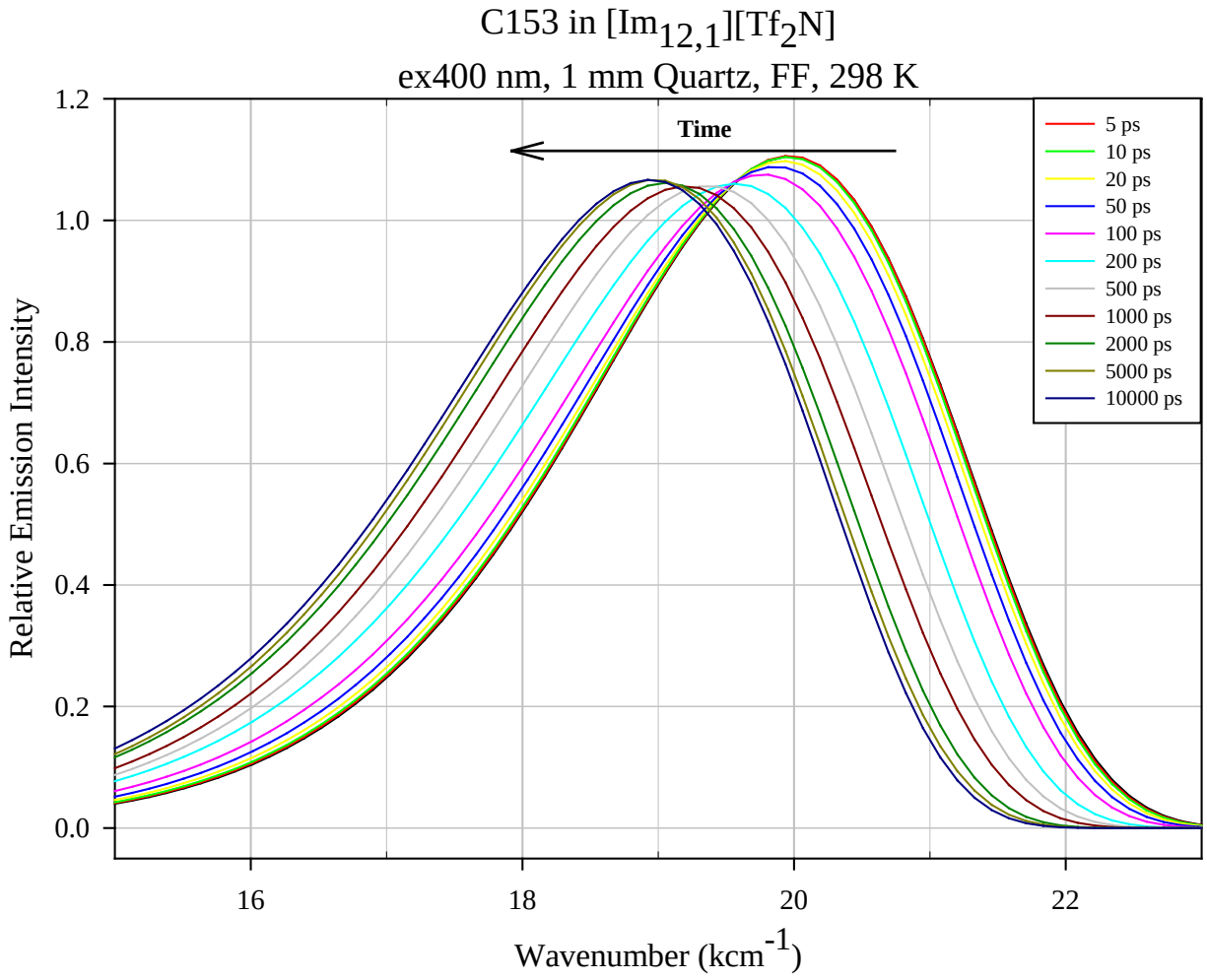

Figure 24: Lognormal fits of reconstructed spectra of C153 in [$Im_{12,1}$][Tf_2N].

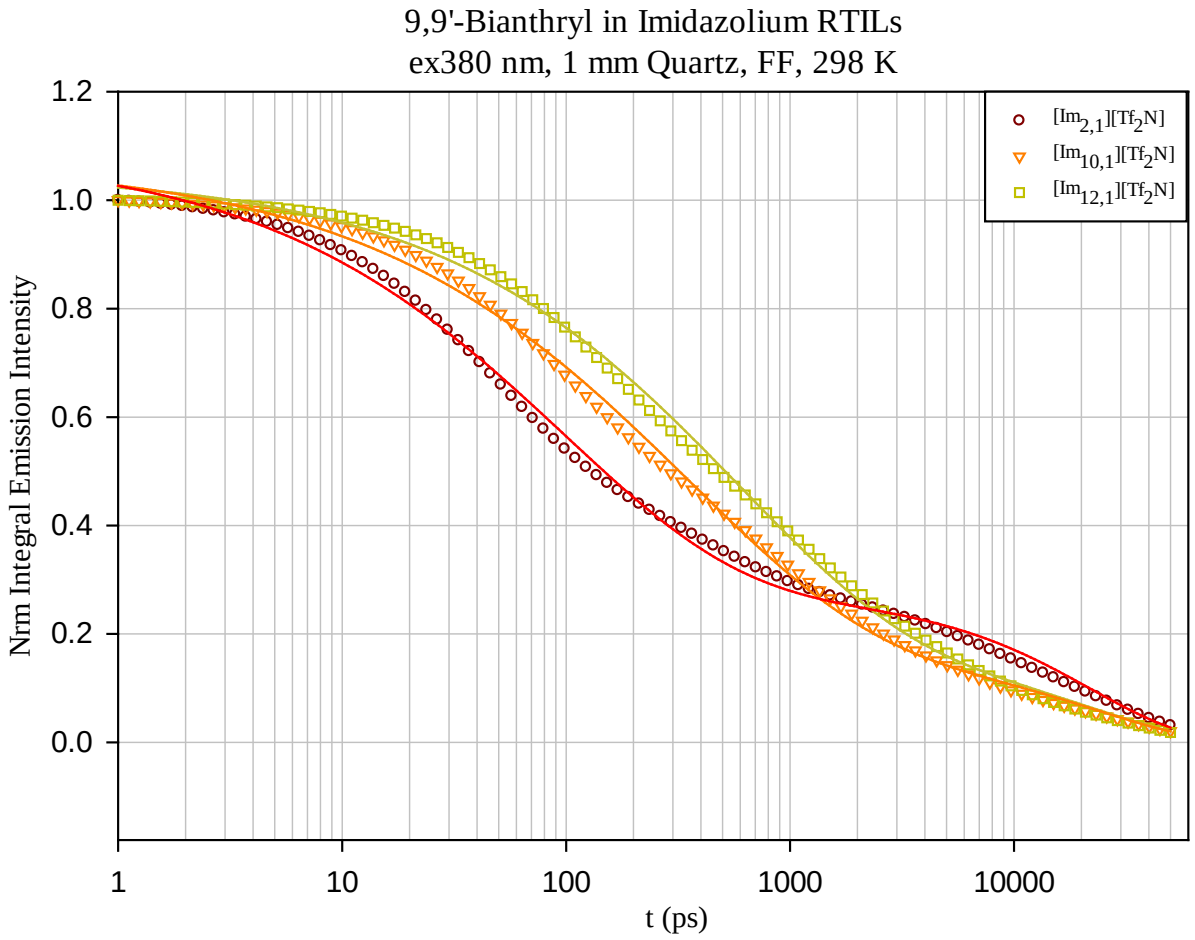

Figure 25: Decay of integral emission intensity of bianthryl in the imidazolium based ionic liquids. The plots have been normalized for ease of comparison. The data are shown by the open symbols and the fits to Eqn. 4 by the solid lines.

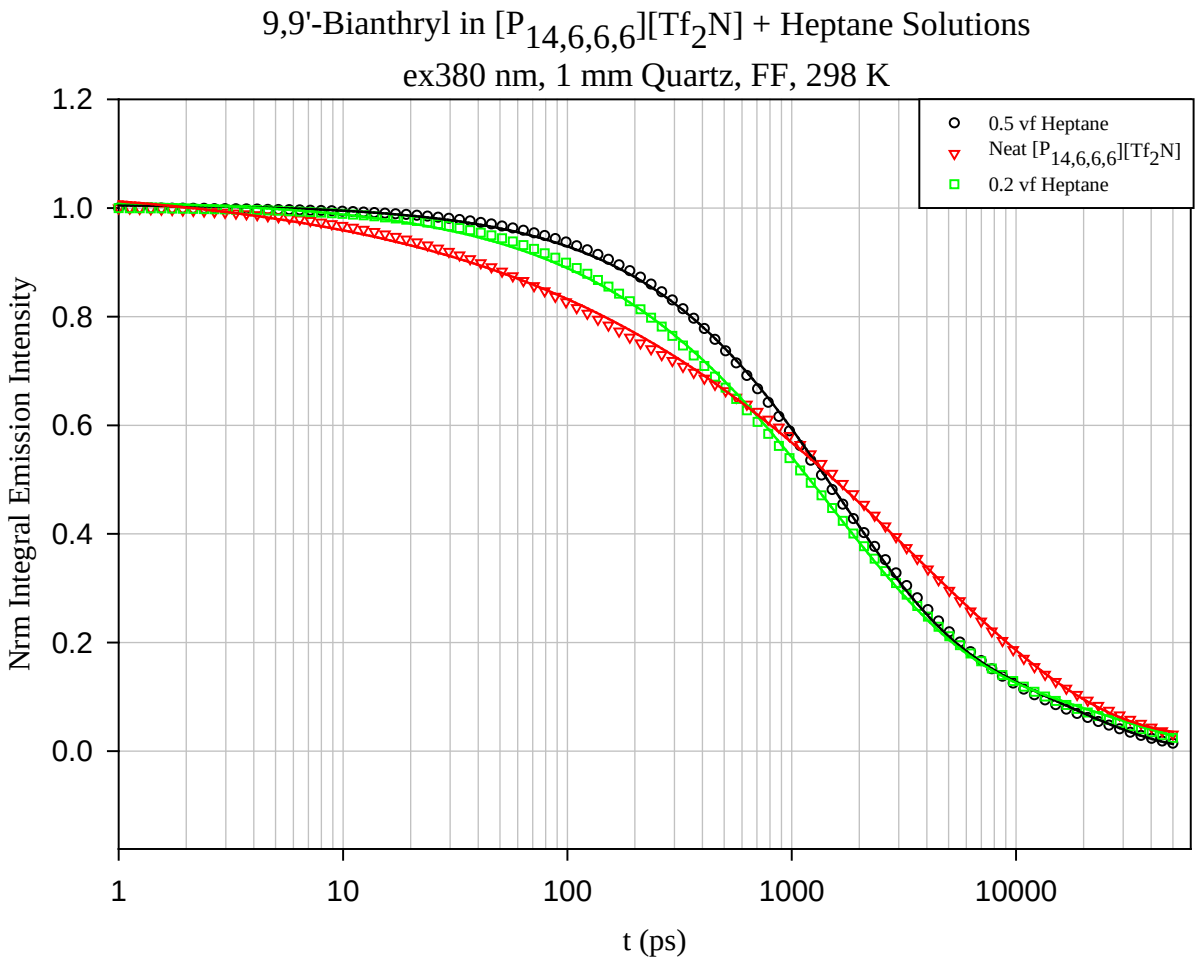

Figure 26: Normalized decays of integral emission intensity of bianthryl in $[P_{14,6,6,6}][Tf_2N]$ and heptane solutions. Open symbols are experimental data and solid lines are fits.

Solvation dynamics decays (i.e. C153 TCSPC data) were fit in upcvfit using the same procedure as for the bianthryl data. To obtain solvation times from these data, and to obtain the Stokes shift time of bianthryl, the integral frequency was plotted as a function of time and the plot fit to a stretched exponential function of the form:

$$\nu(t) = \nu(\infty) + \Delta\nu \cdot exp\left(-\left(\frac{t}{\tau_{solv}}\right)^{\beta}\right) \quad (5)$$

where ν(∞) is the frequency at time infinity, Δν is the Stokes shift between time zero and time infinity, τ_{solv} is the solvation time, and β is the stretching parameter. The integral solvation times $\langle\tau_{\Delta\nu}\rangle$ obtained are calculated in the same manner as the intensity decay times. Solvation times for ionic liquid solvents obtained in this way are also summarized and compared to reaction times in Table 2.

Table 1: Parameters Generated by Fitting Integrated Emission Intensity Decay and Dynamic Stokes Shift to Equations 4 and 5.
λ_{ex} = 380 nm, T = 298 K, All Times in ps

	Intensity Decay						Dynamic Stokes Shift			
	a_1	τ_1	β	$\langle\tau_{rxn}\rangle$	a_2	$\tau_2/10^3$	$\nu\infty$ (kcm^{-1})	$\Delta\nu$ (kcm^{-1})	β	$\tau_{\Delta\nu}$
$[Im_{2,1}][Tf_2N]$	0.753	97	0.55	165	0.247	22	20.125	1.665	0.62	180
$[Im_{10,1}][Tf_2N]$	0.858	340	0.51	656	0.142	25	20.71	1.398	0.52	3200
$[Im_{12,1}][Tf_2N]$	0.853	570	0.55	970	0.147	25	20.327	1.182	0.4	1900
0.5 vf C7 / $[P_{14,6,6,6}][Tf_2N]$	0.789	1500	0.85	1632	0.211	18	20.939	2.055	0.87	6000
0.2 vf C7 / $[P_{14,6,6,6}][Tf_2N]$	0.851	1400	0.7	1772	0.149	30	21.004	2.13	0.73	7100
$[P_{14,6,6,6}][Tf_2N]$	0.145	1800	0.49	3739	0.855	30	19.3	3.792	0.42	200000

Table 2: Solvation Data from C153 as Obtained by Fitting to Eqn. 5. Comparison with Stokes Shift Time and Average Reaction Time of Bianthryl.
All Times are in ps

	τ_{solv}	β	$\langle\tau_{solv}\rangle$	$\frac{BA}{\langle\tau_{\Delta\nu}\rangle}$	$\langle\tau_{rxn}\rangle$
$[Im_{2,1}]$	117	0.75	140[a]	179	165
$[Im_{10,1}]$	690	0.5	1370[b]	3205	662
$[Im_{12,1}]$	1130	0.63	1594	1945	974
0.5 vf C7/$[P_{14,6,6,6}]$	1149	0.64	1595	6020	1648
0.2 vf C7/$[P_{14,6,6,6}]$	1051	0.70	1329	7068	1801
$[P_{14,6,6,6}]$	3720	0.42	11000[c]	204981	3806

a.) From Ref. 10; b.) Measured by Min Liang; c.) Measured by Naoki Ito

4. Discussion of Results and Relation to RTIL structure

In some cases, the dynamics of an electron transfer reaction in solution are strongly correlated to the solvation time of the solvent.[21] This is because an important driving force of such reactions is the fluctuation in the solvent polarization with respect to the charge distribution of the reactant(s), allowing it to access a lower energy region of its energy surface. In probes such as bianthryl which have little (~k_BT) or no activation barrier[22], the dynamics of the solvent orientational relaxation, being much slower than any intramolecular modes involved, become the rate limiting process. In such cases the solvent polarization is taken to be the electron transfer reaction coordinate.[11,23,24] A feature of systems in which the reaction coordinate may be defined as the solvent polarization (and the process is barrierless), is that the lifetime of the electron transfer reaction is typically very close to the solvation time, as may be seen by plotting the reaction time versus the solvation time (see Figure 27). Also depicted are data previously collected by other workers, again correlating the bianthryl reaction lifetime to the solvation time, but for conventional solvents.[25,26,27] The most striking feature of the data shown in Figure 27 is that the ionic liquids closely follow the same trend as the conventional solvents. This would seem to indicate, as with the anthracene shifts, that the bianthryl is experiencing what may most likely be characterized as a highly polar conventional solvent environment. Furthermore the observed effects of the ionic liquid environment on the intramolecular electron transfer reactions seem to be consistent with previous work regarding bimolecular reactions, which suggested that the IL environment did not yield results that varied significantly from conventional solvents of comparable polarity and viscosity.[28]

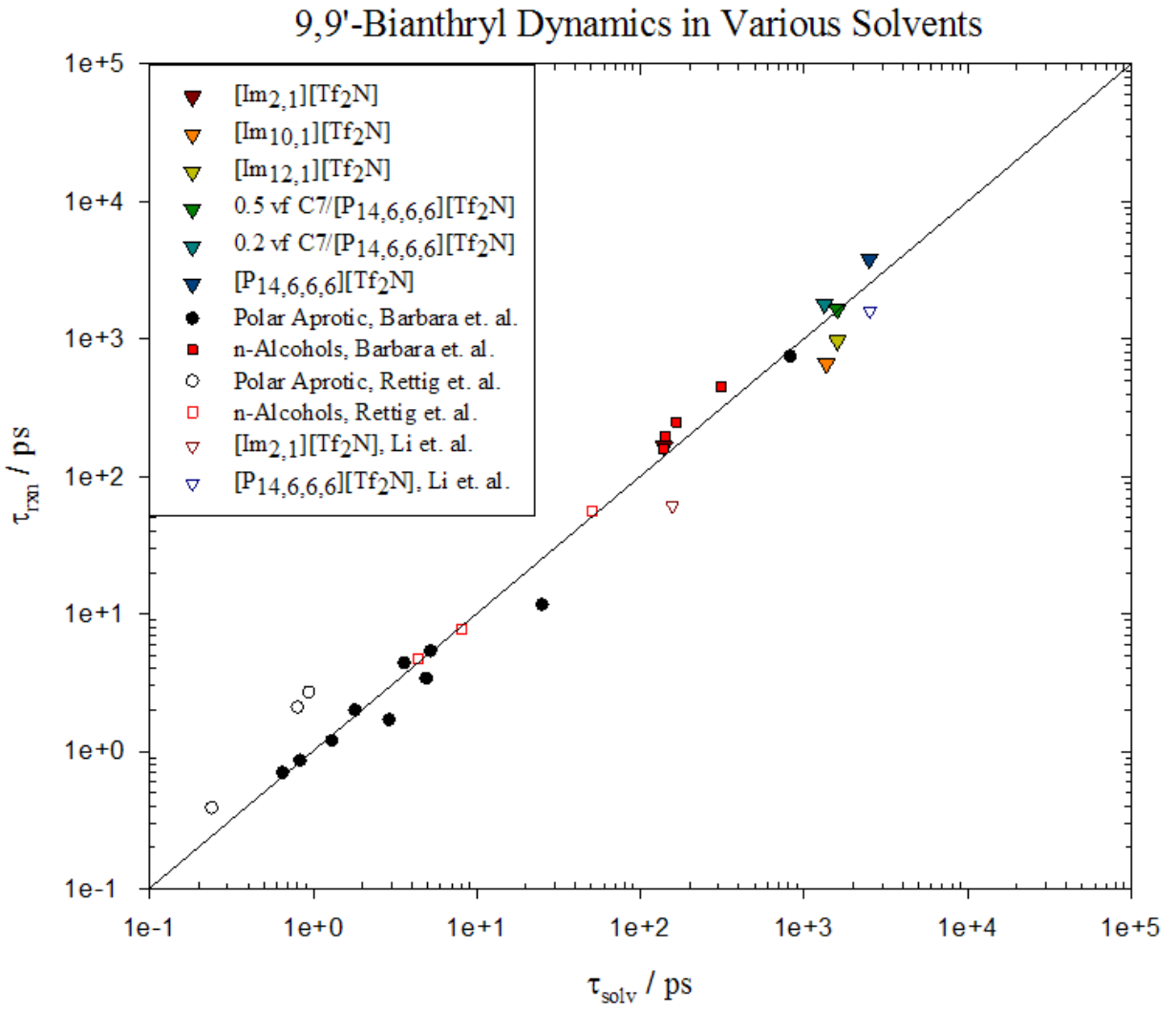

Figure 27: Plot of bianthryl reaction time in a variety of solvents versus the solvation times for those solvents. All ionic liquid ET data are at 298 K except the [$P_{14,6,6,6}$] point (dark blue open triangle) from Li et. al.,which is at 318 K. Conventional solvent data are from refs 13, 14, and 15. This figure is a modified version of Fig. 14 in Ref. 7.

Conclusions

The bianthryl electron transfer dynamics in RTILs measured in this study appear to be consistent with previous measurements in these systems; and both the bianthryl dynamics and the anthracene shifts show strong agreement with their respective trends in conventional solvents. Based on these observations, there is little to suggest that either solute senses anything qualitatively distinctive in ionic liquids compared to polar conventional solvents. These results may at first appear to be at odds with a fairly substantial body of literature from simulation and from other experimental studies which do consistently seem to indicate the presence of structure in certain neat ionic liquids. While it is reasonable to trust the findings of computational studies and scattering experiments on neat ionic liquids, it is not necessarily the case that the structures found in these studies correspond directly to the structure that would be experienced by a solute dissolved in such an IL, or that the structure in either case would be sufficient to present an environment that is significantly different from a highly polar conventional solvent.

One relevant consideration is the fact that a solute such as anthracene or bianthryl will induce a certain degree of structure around itself simply due to the preferential interaction with nonpolar moieties in the liquid. Presented with an ionic liquid that has the potential to form large alkane-like regions, anthracene and bianthryl would presumably be preferentially solvated in these domains. In the case that bianthryl were embedded in such a domain, the expectation would be that the observed electron transfer time would be longer than the solvation time, likely due to the requirement for diffusion of the probe to a more polar region of the liquid for the reaction to occur. Similarly, an anthracene solvated in a sufficiently extensive nonpolar domain, would experience different dielectric properties. As such, the bathochromic shift would be expected to deviate from the trend predicted in Eqn. 1.

Based on the data collected in this study, it cannot be stated that any structure present in long-chain imidazolium-based ionic liquids, or in solutions of $[P_{14,6,6,6}][Tf_2N]$ and heptane is sufficiently large with respect to anthracene or bianthryl to affect their photophysical/chemical behavior in the manner

discussed above. This work however is by no means exhaustive, and it is conceivable that more spectroscopic studies of solute molecules in ionic liquids could do much to assess the strength of this tentative conclusion.

References:

(1) Lopes, J.; Padua, A. *J. Phys. Chem. B* **2006**, *110*, 3330-3335.

(2) Kufo, M.; Michihiro, N.; Ueki, T.; Kitazawa, Y.; Nakamura, Y.; Sawamura, S.; Watanabe, M.; Yamamuro, O. *J. Phys. Chem. B* **2013**, *117*, 2773-2781.

(3) Fujii, K.; Kanzaki, R.; Takamuku, T.; Kameda, Y.; Kohara, S.; Kanakubo, M.; Shibayama, M.; Ishiguro, S.; Umebayashi, Y. *J. Chem. Phys.* **2011**, *135*, 244502.

(4) Russina, O.; Triolo, A.; Gontrani, L.; Caminiti, R. *J. Phys. Chem. Lett.* **2012**, *3*, 27.

(5) Triolo, A.; Russina, O.; Fazio, B.; Triolo, R.; Di Cola, E. *Chem. Phys. Lett.* **2008**, *457*, 362.

(6) Hardacre, C.; Holbrey, J.D.; Mullan, C.L.; Youngs, T.G.A.; Bowron, D.T. *J. Chem. Phys.* **2010**, *133*, 074510.

(7) Annapuredy, H.V.R.; Kashyap, H.K.; DeBiase, P.M.; Margulis, C.J. *J. Phys. Chem. B* **2010**, *114*, 16838.

(8) Yang, P.; Voth, G. A.; Xiao, D.; Hines, L. G.; Bartsch, R. A.; Quitevis, E. L. *J. Chem. Phys.*, **2011**, *135*, 034502.

(9) Lewis, J.E.; Biswas, R.; Robinson, A.G.; Maroncelli, M. *J. Phys. Chem. B*, **2001**, *105*, 3306.

(10) Coutinho, Joao A.P. and Gardas, Ramesh L. Predictive Group Contribution Models for the Thermophysical Properties of Ionic Liquids. In *Ionic Liquids: From Knowledge to Application*; Plechkova, N.C|V., Rogers, R.D., Seddon, K.R., Eds.; ACS Symposium Series 1030; American Chemical Society: Washington, DC, 2009; pp385-401.

(11) Li, X.; Liang, M.; Chakraborty, A.; Kondo, M.; Maroncelli, M. *J. Phys. Chem. B* **2011**, *115*, 6592.

(12) (a) Catalan, J.; Lopez, V.; Perez, P. *J. Fluor.* **1996**, *6*, 15.
(b) Schneider, F.; Lippert, E. *Ber. Bunsenges. Phys. Chem.* **1968**, *72*, 1155.

(13) Bagchi, Biman. Orientational and Dielectric Relaxation. In *Molecular Relaxation in Liquids*; Oxford: New York, 2012; pp 51-77.

(14) McQuarrie, Donald A. The Time-Correlation Function Formalism, I. In *Statistical Mechanics*; University Science Books: Mill Valley, CA, 2000; pp 495-499.

(15) Tariq, M.; Forte, P.A.S.; Costa Gomes, M.F.; Canongia Lopes, J.N.; Rebelo, L.P.N. *J. Chem. Thermodynamics*, **2009**, *41*, 790.

(16) Mac, M.; Milart, P.; Kwiatkowski, P.; Tokarczyk, B. *J. Lumin.*, **1999**, *81*, 199.

(17) Lewis, J.E.; Maroncelli, M. *Chem. Phys. Lett.*, **1998**, *282*, 197.

(18) Koti, A.S.R.; Periasamy, N. *J. Chem. Phys.* **2001**, *115*, 7094.

(19) Fee, R.S.; Maroncelli, M. *Chem. Phys.* **1994**, *183*, 235.

(20) Berberan-Santos, M.N.; Bodunov, E.N.; Valeur, B. *Chem. Phys.* **2005**, *315*, 171.

(21) Bagchi, Biman. Electron-Transfer Reactions. In *Molecular Relaxation in Liquids*; Oxford: New York, 2012; pp 195-225.

(22) Tominaga, K.; Walker, G.C.; Kang, T.J.; Fonseca, T.; Barbara, P.F. *J. Phys. Chem.* **1991**, *95*, 10485.

(23) Rasaiah, Jayendran C.; Zhu, Jianjun. *J. Chem. Phys.* **2008**, *129*, 214503.

(24) Heitele, Hans. *Angew. Chem. Int. Ed. Engl.* **1993**, *32*, 359.

(25) Kang, T.J.; Kahlow, M.A.; Giser, D.; Swallen, S.; Nagarajan, V.; Jarzeba, W.; Barbara, P.F. *J. Phys. Chem.* **1988**, *92*, 6800

(26) Kang, T.J.; Jarzeba, W.; Barbara, P.F.; Fonseca, T. *Chem. Phys.* **1990**, *149*, 81.

(27) Kovalenko, S.A.; Lustres, J.L.P.; Ernsting, N.P.; Rettig, W. *J. Phys. Chem. A* **2003**, *107*, 10228.

(28) Koch, M.; Rosspeinter, A.; Angulo, G.; Vauthey, E. *J. Am. Chem. Soc.* **2012**, *134*, 3729.

Appendix:
Input file for *stokes_analysis* reconstruction of bianthryl decays in [$Im_{12,1}$][Tf_2N]

```
33
Bianthryl / Im121Tf2N : 11Jun2013
FF 12.2ps / channel

## ne  chi2     scale   bck     tsft     a1      a2      a3      a4     t1(ps)    t2(ps)    t3(ps)    t4(ps)
 1 14  1.01 0.9356E+04    0.  12.196   0.508   0.324   0.138   0.030   117.317   794.259  3594.412 23436.646
 2 14  1.02 0.8150E+04    0.  12.043   0.512   0.310   0.145   0.033   119.740   851.951  3848.669 22226.584
 3 14  1.02 0.8185E+04    0.  14.570   0.481   0.326   0.156   0.037   108.614   805.708  3863.534 22716.795
 4 14  1.06 0.8346E+04    0.  12.283   0.483   0.307   0.168   0.042   133.943   942.443  4313.363 22280.658
 5 14  1.01 0.7944E+04    0    9.516   0.393   0.367   0.183   0.057   121.161   880.070  3465.528 29741.537
 6 14  1.02 0.7567E+04    0.  14.150   0.420   0.341   0.182   0.056   133.037   969.597  4206.320 24626.592
 7 14  1.08 0.9282E+04    0.   9.610   0.409   0.334   0.192   0.066   112.796   910.538  3931.961 26133.195
 8 14  1.00 0.7488E+04    0.  14.987   0.403   0.321   0.201   0.074   128.783   977.079  4211.542 25871.150
 9 14  1.04 0.7991E+04    0.  12.774   0.370   0.324   0.214   0.091   129.889   961.136  4036.654 27577.582
10 14  1.10 0.8215E+04    0.   9.765   0.353   0.323   0.216   0.108   126.995  1041.176  4164.489 27907.475
11 14  1.10 0.7302E+04    0.  11.410   0.386   0.298   0.215   0.101   133.216   988.771  4236.066 26055.652
12 14  1.11 0.7934E+04    0.   9.402   0.319   0.305   0.231   0.145   130.858  1009.127  4059.386 28491.662
13 14  1.09 0.6959E+04    0.  12.501   0.343   0.294   0.227   0.136   157.845  1103.455  4436.783 27500.807
14 14  1.05 0.7680E+04    0.   9.681   0.322   0.279   0.233   0.166   110.288   920.729  4082.020 28606.578
15 14  1.06 0.7665E+04    0.  10.348   0.347   0.289   0.224   0.140   113.166   898.994  4237.213 27040.316
16 14  1.07 0.7079E+04    0.  12.998   0.307   0.278   0.244   0.171   134.211   959.190  4270.161 27529.635
17 14  1.07 0.7681E+04    0.   8.760   0.322   0.254   0.222   0.202   115.263   996.331  4217.475 28807.926
18 14  1.12 0.7379E+04    0.   8.050   0.221   0.249   0.238   0.293   123.920  1107.147  4330.414 29935.953
19 14  1.11 0.7408E+04    0.  15.244   0.313   0.264   0.234   0.189   110.761   943.338  4368.620 27637.660
20 14  1.11 0.7429E+04    0.  11.305   0.321   0.273   0.215   0.191   149.989  1150.611  4936.055 28422.717
21 14  1.10 0.6902E+04    0.  10.458   0.288   0.254   0.212   0.246    91.443   961.803  4663.472 29442.143
22 14  1.09 0.7044E+04    0.   9.342   0.289   0.239   0.215   0.256   128.070  1037.408  4799.155 29139.865
23 14  1.08 0.7450E+04    0.  14.435   0.308   0.253   0.244   0.194   160.655  1101.497  4816.037 26439.932
24 14  1.02 0.6897E+04    0.  11.362   0.327   0.270   0.250   0.153   145.524  1161.350  5085.992 25257.906
25 14  1.01 0.6933E+04    0.  11.698   0.295   0.261   0.272   0.172   164.001  1201.440  5074.557 25502.168
26 14  1.08 0.6822E+04    0.   8.652   0.252   0.193   0.211   0.344   126.483  1180.157  5412.602 30567.965
27 13  1.15 0.6127E+04    0.  10.807   0.419   0.387   0.194   0.000   514.723  4126.125 22858.516     0.000
28 13  1.21 0.6533E+04    0.   9.302   0.404   0.353   0.244   0.000   498.154  4057.260 25823.258     0.000
29 13  1.12 0.6147E+04    0.  15.044   0.431   0.405   0.165   0.000   545.459  4107.403 20079.268     0.000
30 14  1.07 0.8932E+04    0.  11.603   0.271   0.270   0.244   0.215   189.443  1244.665  5383.209 29365.279
31 14  0.99 0.6718E+04    0.  21.938   0.296   0.291   0.305   0.108   211.641  1360.048  5206.929 20732.252
32 14  1.00 0.5853E+04    0.  23.843   0.307   0.312   0.285   0.097   244.592  1436.382  5414.737 22016.502
33 14  1.03 0.3958E+04    0.  35.287   0.315   0.290   0.302   0.093   302.664  1434.187  5100.061 19280.55

1   405.0  11  1.2618E+3      50000       28000
2   410.0  11  1.6063E+3      50000       28000
3   415.0  11  2.0619E+3      50000       28000
```

4	420.0	11	2.3433E+3	50000	28000
5	425.0	11	2.5206E+3	50000	28000
6	430.0	11	2.7512E+3	50000	28000
7	435.0	11	2.9956E+3	50000	28000
8	440.0	11	3.2446E+3	50000	28000
9	445.0	11	3.4518E+3	50000	28000
10	450.0	11	3.5935E+3	50000	28000
11	455.0	11	3.6816E+3	50000	28000
12	460.0	11	3.7235E+3	50000	28000
13	465.0	11	3.7771E+3	50000	28000
14	470.0	11	3.7480E+3	50000	28000
15	475.0	11	3.6233E+3	50000	28000
16	480.0	11	3.5198E+3	50000	28000
17	485.0	11	3.3486E+3	50000	28000
18	490.0	11	3.1358E+3	50000	28000
19	495.0	11	2.9397E+3	50000	28000
20	500.0	11	2.7567E+3	50000	28000
21	510.0	11	2.2867E+3	50000	28000
22	520.0	11	1.8856E+3	50000	28000
23	530.0	11	1.5145E+3	50000	28000
24	540.0	11	1.2052E+3	50000	28000
25	550.0	11	9.3209E+2	50000	28000
26	560.0	11	7.1989E+2	50000	28000
27	570.0	11	5.5971E+2	50000	28000
28	580.0	11	4.2108E+2	50000	28000
29	590.0	11	3.3031E+2	50000	28000
30	600.0	11	2.4344E+2	50000	28000
31	620.0	11	1.4116E+2	50000	28000
32	640.0	11	7.4870E+1	50000	28000
33	660.0	11	4.4000E+1	50000	28000